








Research Article

Strain Partitioning along Terrane Bounding and Intraterrane Shear Zones: Constraints from a Long-Lived Transpressional System in West Gondwana (Ribeira Belt, Brazil)

F. M. Faleiros ¹, B. V. Ribeiro ², G. A. C. Campanha ¹, P. A. Cawood ²,
D. I. G. Cabrita ¹, M. T. A. G. Yogi³, L. A. Milani¹, D. V. Lemos-Santos¹, V. V. Almeida ⁴,
S. W. O. Rodrigues⁵, I. S. Malta⁶, and A. J. Forero-Ortega ⁷

¹Department of Mineralogy and Geotectonics, University of São Paulo, Rua do Lago 562, 05508-900 São Paulo, SP, Brazil

²School of Earth, Atmosphere and Environment, Monash University, Clayton, Victoria 3800, Australia

³Department of Earth Sciences, Carleton University, 1125 Colonel By Drive, Ottawa, ON, Canada K1S 5B6

⁴Geodynamics Division, Geological Survey of Brazil (CPRM), Rua Costa 55, 01304-010 São Paulo, SP, Brazil

⁵Faculdade de Ciências e Tecnologia, Universidade Federal de Goiás (UFG), Rua Mucuri, S/n-Setor Conde dos Arcos, 74968-755 Aparecida de Goiânia, GO, Brazil

⁶Département de Géologie et Génie Géologique, Université Laval, Québec, Canada G1V 0A6

⁷Institute for Geophysics, Pontificia Universidad Javeriana, Bogotá, Colombia

Correspondence should be addressed to F. M. Faleiros; ffalei@usp.br

Received 5 October 2021; Accepted 30 December 2021; Published 10 February 2022

Academic Editor: Sayandeep Banerjee

Copyright © 2022 F. M. Faleiros et al. Exclusive Licensee GeoScienceWorld. Distributed under a Creative Commons Attribution License (CC BY 4.0).

Shear zones are zones of localized high strain accommodating differential motion in the lithosphere and impacting the crustal rheology and deformational history of orogenic belts. Although terrane bounding shear zones are widely studied, intraterrane shear zones and their tectonic significance, especially in association with supercontinent assembly, is a largely unexplored topic. The Ribeira Belt (SE Brazil), a Neoproterozoic-Cambrian orogenic belt from West Gondwana, is dissected by a crustal-scale NE-trending transcurrent shear zone system that juxtaposes composite terranes. Despite its extensive coverage and complexity, this shear zone system remains poorly investigated. In this paper, we explore the thermal and deformational regimes, and timing of ductile shearing using a multiscale approach combining structural analysis derived from remote sensing and field-based structural data, microstructures, quantitative structural analysis, and multiminerall U–Pb geochronology (zircon, titanite, monazite, and xenotime). Our data, combined with previously published data, indicate a transitional northeastward increase in metamorphic conditions from lower greenschist to granulite facies conditions (from 250–300 to 750–800°C), reflecting the different crustal levels that are exposed. Vorticity and finite strain data indicate a complex strain regime with varied contributions of pure and simple shear and oblate-shape ellipsoids in strike-slip shear zones and prolate-shaped ellipsoids in dip-slip reverse shear zones. The strain set suggests that all shear zones were developed under subsimple shear deformational regimes involving thrusting and folding followed by wrench tectonics. The pure shear component of deformation was accommodated in folded domains between shear zones. Geochronological data suggest intermittent ductile shear zone activations from ca. 900–830 to 530 Ma, partially coeval with at least two major episodes of terrane accretion at 850–760 Ma and 610–585 Ma. The spatial and temporal record of shear zones within the Ribeira Belt indicates that some relate to assembly of the belt and represent either terrane bounding structures (e.g., Itapirapuã shear zone) or intraterrane structures (e.g., Ribeira, Figueira, and Agudos Grandes shear zones), whereas others are terrane bounding, postcollisional shear zones (e.g., Taxaquara shear zone) reactivated in an intracontinental setting (560–535 Ma).

1. Introduction

Shear zones are zones of localized high strain that accommodate differential motion in the Earth's crust and mantle, exerting a fundamental control on crustal rheology and deformational evolution of orogenic belts [1–3]. They localize deformation and accommodate movement from the microscale to the orogen scale and include first-order structures at tectonic plate boundaries; for example, the Alpine Fault, New Zealand [4], and the San Andreas Fault, United States of America and Mexico [5]. Shear zone systems are key features in accretionary-to-collisional orogens, materializing sutures and terrane boundaries in regions of orogenic assembly, as well as in postorogenic terrane dispersal [6]. Due to their major tectonic importance, studies of suture and terrane bounding shear zones are common in the literature (e.g., [7, 8]), whereas analysis of intraterrane shear zones and their tectonic significance, especially in association with supercontinent assembly, is a largely unexplored topic.

The Ribeira Belt is a Neoproterozoic-Cambrian NE-trending orogen that occupies a central position in West Gondwana reconstructions (Figure 1(a)), associated with the convergence between Archean-Paleoproterozoic rock assemblages from the São Francisco, Paranapanema, Luís Alves, and Congo cratons (Figures 1(a) and 1(b); [9]). It has been traditionally interpreted as recording a history evolving from accretionary to collisional with its current architecture controlled by a late-collisional, crustal-scale, transcurrent shear zone system that resulted in the juxtaposition of fault-bounded composite terranes in the Ediacaran-Cambrian (e.g., [10–15]). Alternative models have proposed an intracontinental setting for the orogen [16–19], although without taking into account the role of terrane bounding shear zones from the southern and central Ribeira Belt.

The Ribeira Belt presents an anastomosing network of transcurrent shear zones with a first-order structure defined by the combined Lancinha, Cubatão, and Além Paraíba-Pádua shear zones (Figure 1(b)), which can be traced over a total along strike distance of some 2100 km (800 km exposed and 1300 km covered by the Paraná Basin; [20]). Second-order shear zones, including the Ribeira, Morro Agudo, Agudos Grandes, and Caucaia shear zones (Figure 1(c)), further divide the Ribeira Belt into a series of lenticular-shaped blocks of discrete lithotectonic units (terranes) that are themselves further segmented by third-order intraterrane shear zones. Previous research on the shear zones has focused on aspects of individual structures, including textural analyses and grain-scale deformation mechanisms [21–26], fluid flow and vein development [27–29], and field-based structural analysis, strain quantification, and thermobarometry [15, 25, 30, 31]. Geochronological studies are scarce and performed only in a few individual terrane bounding shear zones [14, 30, 32–37]. The available data indicate a long-lived and poorly understood evolution for the shear zone system extending from 610 to 530 Ma, with a few data indicating brittle activities during the Paleozoic [38]. Geochronology, structural analysis, and strain quantifications of intraterrane shear zones are scarce, and their relationships with terrane boundary shear

zones have received only limited investigation. Recent published geochronological data indicate that some geological units from the southern Ribeira Belt record evidence for a compressional metamorphic event at 850–760 Ma [39, 40], raising the possibility that some deformational structures and shear zones could have been formed during the Tonian.

This paper investigates the role of the terrane boundaries and intraterrane shear zones in the southern Ribeira Belt through a multiscale structural analysis derived from remote sensing and field-based structural analysis, coupled to microstructures, quantitative structural data (finite strain and kinematic vorticity), and multiminerall U–Pb geochronology. These data allow us to discuss the microstructural, thermal, and deformational regimes of this shear zone system and also the timing of ductile shearing. When combined to existing data from the literature, these shear zones record a complex long-lived strain regime.

2. Tectonic Framework

The Ribeira Belt comprises a complex assemblage of tectonostratigraphic terranes of contrasting lithological character, ages, and tectonic settings bounded by shear zones with reported ages largely in the range of Ediacaran to Cambrian (610–530 Ma; Figure 1(c); [10, 12–15, 33, 34, 37, 39–44]). Contacts between the Ribeira Belt and the bounding Paranapanema, Luís Alves, and Congo cratons are largely concealed, while the southern margin of the São Francisco Craton is in contact with the Passos, Socorro, and Guaxupé nappes from the southern Brasília Belt (Figures 1(a) and 1(b)). This lack of exposed contacts with enclosing cratons has hindered the unravelling of the tectonic evolution of the belt. The southern Brasília Belt extends for c. 800 km along the southwestern margin of the São Francisco Craton, being segmented into west-verging nappes related to the convergence with the Paranapanema Craton [45]. Collisional tectonics (650–630 Ma), exhumation of high-pressure nappes and eclogites (610–605 Ma), and final cooling (600–580 Ma) took place relatively early when compared to the Ribeira Belt [45]. The contact with the Paranapanema Craton, the main cratonic reference to the southern and central portions of the Ribeira belt, is concealed by Paleozoic sedimentary rock units from the Paraná Basin (Figures 1(b) and 1(c)), with its position delineated by geophysical studies and deep borehole data [46]. The Congo craton is preserved in present-day Africa, and its eastern boundary is covered by Phanerozoic sedimentary rocks, precluding direct comparison with the Brazilian counterpart. The Luís Alves Terrane (Figures 1(b) and 1(c)) is a small cratonic remnant composed of Archean-Paleoproterozoic granulitic gneisses (2.7–2.0 Ga.; [47, 48]), with K–Ar hornblende and biotite ages between 2100 and 1700 Ma, indicating that it was not reworked during the Brasiliano/Pan-African Orogeny [49].

The Lancinha-Cubatão-Além Paraíba-Pádua strike-slip shear zone represents the main tectonic boundary within the orogen (Figure 1(c)). In the southern Ribeira Belt, this composite shear zone separates terranes with metasedimentary rock assemblages of Mesoproterozoic to early Tonian depositional ages to the north (Apiaí and Embu terranes;

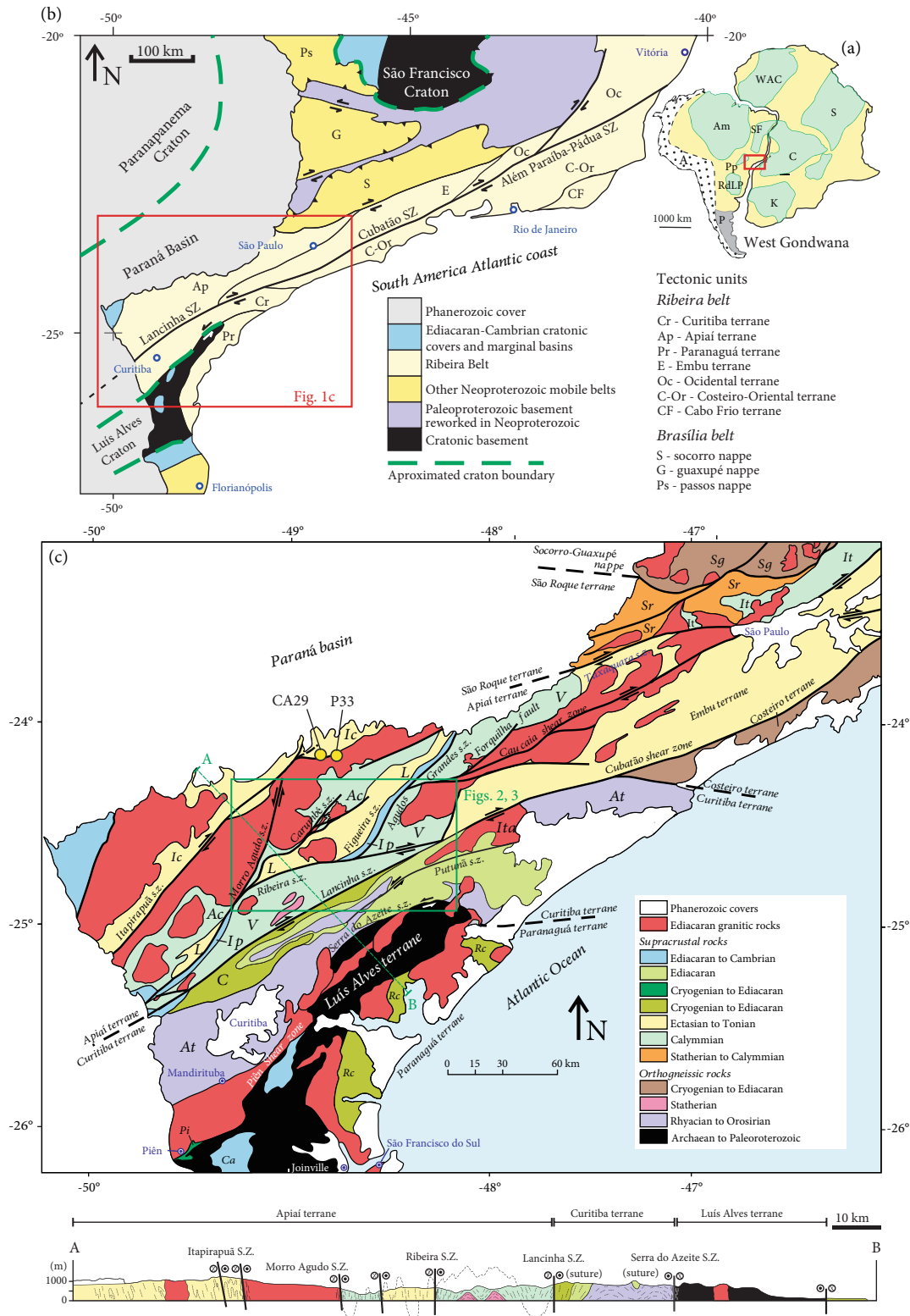


FIGURE 1: (a) Simplified West Gondwana reconstruction. (b) Regional geological context of south-southeastern Brazil with the location of the Ribeira Belt indicated by the red rectangle (adapted from Faleiros et al. [15]). (c) Simplified geotectonic map of the southern and central portions of the Ribeira Belt with the location of the study area and of the samples CA29 and P33 (modified from Ricardo et al. [41]). Geological units: Itaiacoca Group (Ic), Água Clara Formation (Ac), Lajeado Group (L), Votuverava Group (V), São Roque Group (Sr), Serra do Itaberaba Group (It), Iporanga Formation (Ip), Socorro-Guaxupé Nappe (Sg), Capiru Formation (C), Turvo-Cajati Formation (TCF), Itapeúna Suite (Ita), Piên Mafic-Ultramafic Suite (Pi), Rio das Cobras Formation (Rc), and Atuba Complex (At). The maps use geographical coordinates in degrees (WGS-84 datum).

Figure 1(b)) from terranes with Ediacaran depositional ages (Curitiba and Costeiro-Oriental terranes; Figure 1(b)) to the south [16, 41, 43, 44]. Ediacaran granites associated with accretionary to postcollisional settings (ca. 630–560 Ma) are emplaced across the belt, cutting all terranes (Figure 1(c)) (e.g., [50–54]).

The Apiaí Terrane (Figures 1(c) and 2), the focus of this paper, is primarily composed of metasedimentary rock assemblages, with restricted basement rocks dominated by orthogneiss with zircon U–Pb ages between ca. 1780 and 1740 Ma that outcrop in the cores of broad antiforms, with subordinate Rhyacian rocks (ca. 2200 Ma) [55].

The metasedimentary rock assemblages are grouped into five major fault-bounded units of distinct ages and tectonic settings (Figure 1(c)): Água Clara Formation (1590–1470 Ma), Votuverava Group (1490–1470 Ma), Lajeado Group (1200–880 Ma), Itaiacoca Group (1030–910 Ma), and Iporanga Formation (590–580 Ma) (Figure 1(c); [42–44, 56–59]). Metamorphic conditions vary from lower greenschist (chlorite zone) to amphibolite facies (kyanite zone) with medium pressure (6–9 kbar) regime [22, 29, 58]. Ediacaran (630–560 Ma) granites intruded all units from the Apiaí Terrane (e.g., [50–54]).

3. Analytical Methods

3.1. Isogon Patterns. The isogon method generates lines joining points of equal orientation of a foliation within a lithotectonic unit (Ramsay, 1967). For a heterogeneous simple shear zone, the isogons should be subparallel to the shear zone walls, as the foliation initially develops at an angle of 45° in relation to the zone, which decreases progressively towards the shear zone interior (higher strain), although theoretically never reaching 0° [1, 60]. In transpressional zones, the initial angles of the mylonitic foliation in relation to the shear zone should be lower than 45°, and higher values are predicted for transtensional zones (e.g., [61–64]). Distinct angular relationships are possible for shear zones affecting a preexisting fabric. We traced the foliation trajectories from 1:60,000 scale aerial photographs and satellite images, and an isogon map was elaborated taking as reference the mean orientation of the Ribeira shear zone (N80°E).

3.2. Finite Strain Quantification. Shape-preferred orientation (SPO) determinations were carried out in eight oriented samples including five samples of fine-grained metasedimentary rocks and three metaconglomerate rock samples. SPO results can be associated with the finite strain tensor if the initial shape of the deformed objects was approximately equidimensional, and there was no viscosity contrast between the measured objects and their enveloping matrix. For three metaconglomerate samples, clasts of three mutually orthogonal sections were manually traced and then captured in raster format by a scanner. In the case of fine-grained mylonitic rock samples, thin section photomicrographs were captured by a CCD camera coupled to a petrography microscope. Thus, the fine-grained clasts were digitized using CorelDraw® software. The images were converted in raster format, whereby 2D shape quadratic tensors [65] of

deformed objects were calculated and the corresponding strain ellipses with their respective long and short axes were deduced by the inertia tensor method [65] using the SPO software [66, 67].

The calculated sectional subsets (ellipses) were integrated with the ELLIPSOID software [66] to calculate the 3D ellipsoid, the orientation of its principal axes (X , Y , and Z), and the shape parameters. The software calculates an “incompatibility index” ($\sqrt{F}\%$), which measures the compatibility or misfit between the sectional ellipses (2D) and the calculated 3D ellipsoid [68]. This parameter also establishes if the sectional ellipses lead to a 3D hyperboloid rather than an ellipsoid [67]. The fit is considered good if $\sqrt{F} < 10\%$ and, it is ideal when values are $\sqrt{F} = 0\%$ [67]. The ellipsoid shape is described by the T parameter, when $T \sim 0$ ($X/Y = Y/Z$) the shape is planar-linear (plane strain), $T < 0$, ($X > Y = Z$) it is linear or prolate and $T > 0$ ($X = Y > Z$) the shape is planar or oblate. The anisotropy intensity can be represented by the X/Z ratio or the anisotropy degree parameter, P' , which ranges from 1 upwards (sphere to ellipsoid; 1 to ∞) [69].

3.3. Kinematic Vorticity Analysis. The noncoaxiality of deformation for a total of 15 tectonite samples cut in the XZ section of the strain ellipsoid (perpendicular to the foliation and parallel to the stretching lineation) was estimated using the mean vorticity number (W_m ; [70]) through two well-known methods: rigid porphyroclast rotation (RP; [71, 72]) and the δ/β -method [72] using the quartz crystallographic-preferred orientation previously published in [22].

For the RP method, porphyroclasts were digitized using the CorelDraw® software with at least 300 grains per sample to ensure a sound statistical representation. These images were processed using the SPO software [66] to calculate the shape ratio and the angle between the major axis and the foliation for each porphyroclast to construct a Wallis plot [72]. This graphic representation allows the determination of the values of critical shape ratio (R_c), below which the objects rotate continuously, and is essential to calculate the mean vorticity number (W_m) using

$$W_m = \frac{R_c^2 - 1}{R_c^2 + 1}. \quad (1)$$

The δ/β -method [72] correlates two geometrical data from quartz crystallographic-preferred orientation (CPO) and its oblique shape-preferred orientation (SPO). These features provide the angle (β) between the shear plane and the principal foliation in quartz [c]-axis CPO and the maximum angle (δ) between quartz oblique fabric and main foliation in the thin section. The mean vorticity number is then calculated using Equation (2) [72].

$$W_m = \sin 2(\delta + \beta). \quad (2)$$

The values of β and δ angles were measured from quartz CPO data using MTEX codes developed in MATLAB

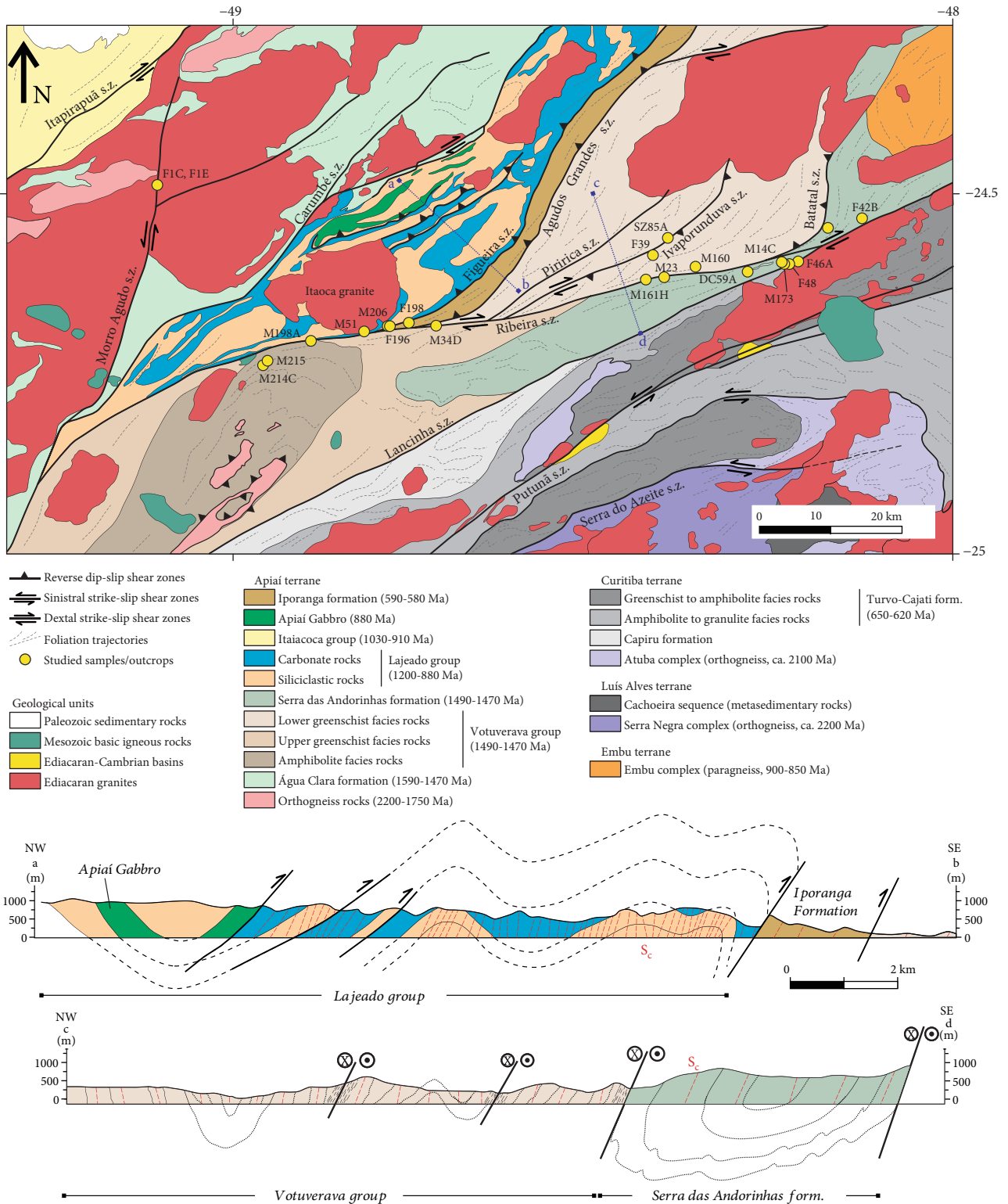


FIGURE 2: Simplified geological map of the study area, showing the studied samples discussed in the text. The map uses geographical coordinates in degrees (WGS-84 datum).

environment [73] and statistically preferred orientation of digitized recrystallized quartz grains analyzed in the SPO software [66].

3.4. *U-Pb Geochronology.* U-Pb isotopic and trace element data of zircon, monazite, xenotime, and titanite were collected at the Isotopia Facility, Monash University (Australia),

TABLE 1: Shear zone groups present in the southern Ribeira Belt based on geometry and kinematics.

| Type | Shear zone group | Sense of shear | Orientation | Examples |
|------|--------------------------|----------------|-------------|---------------------------------------------|
| 1 | NE-trending strike-slip | Dextral | N60E | Lancinha, Cubatão, Caucaia, Itapirapuã |
| 2 | NE-trending dip-slip | Top to SE | N35E | Figueira, Agudos Grandes, Piririca, Batatal |
| 2 | NE-trending dip-slip | Top to NW | N35E | Ivaporunduva |
| 3 | ENE-trending strike-slip | Dextral | N80E | Ribeira |
| 4 | NNE-trending strike-slip | Sinistral | N10E | Morro Agudo |
| 5 | NE-trending strike-slip | Sinistral | N60E | Serra do Azeite, Putunã |

performed via laser ablation split stream inductively coupled plasma mass spectrometer (LASS-ICP-MS) using an ASI RESOLUTION 192 nm laser ablation system coupled to a Thermo Fisher iCAP TQ ICP-MS for measurement of U and Pb isotopes and to a Thermo Fisher iCAP-Q ICP-MS for measurement trace element concentrations. A detailed description of the U–Pb–trace element analytical methods is described elsewhere [33, 34]. Zircon 91500 [74], monazite Madel [75], and titanite BLR [76] were employed as primary standards to calibrate the U–Pb isotopic data. Zircons GJ1 [77], Plešovice [78], OG1 [79], and QGNG [80] were employed as secondary standards and treated as unknowns during zircon U–Pb analyses. Monazite 44069 [81] and titanite OLT [82] were employed as secondary standards and treated as unknowns during monazite/xenotime and titanite U–Pb analyses. All the secondary standards yielded similar results to those from reference values as presented in the supplementary material (available here). The international glass NIST610 was employed as primary standard for trace element analyses, and Si, Ce, and Y were employed as internal standards for titanite, monazite, and xenotime, respectively, considering the stoichiometric molar proportion. NIST612, BCR2, and ATHO were employed as secondary trace element standards and treated as unknowns to evaluate the data reproducibility and accuracy. All standard results agree with recommended values, yielding an accuracy of 1–5% compared to the reference values (see supplementary material (available here)).

Data reduction was performed with Iolite 4 [83, 84] using the in-built U–Pb and trace element data reduction schemes by modelling the down-hole fractionation with a smoothed cubic spline. U–Pb diagrams and final ages were calculated using IsoplotR [85]. Ages and uncertainties are presented with 2σ level of confidence with final ages presented as $x \pm |y|$, with x and $|y|$ representing the age (Ma) and the studentized error stated at 95% confidence, respectively. Common-Pb correction was solely applied for titanite U–Pb data from sample CA29 following procedures described elsewhere [34, 86, 87]. This procedure involves calculating the natural inverse isochron with all reliable data in the Tera-Wasserburg diagram. The lower intercept age is used to calculate the initial $^{207}\text{Pb}/^{206}\text{Pb}$ from the Pb evolution model of Stacey and Kramers [88] with multiple interactions until no further significant change. In this case, the initial $^{207}\text{Pb}/^{206}\text{Pb}$ was established after three interactions. Rare-earth element concentrations were normalized to

chondrite following the reference values from McDonough and Sun [89].

Additional in situ monazite dating from sample M214C (garnet-biotite mylonitic schist) was performed at the Geochronological Research Center of the Institute of Geosciences, University of São Paulo, Brazil, using a Photon-Machines Analyte G2 193 nm excimer laser ablation system coupled with a Thermo Scientific Neptune ICP-MS. The experiments were performed with $7\text{ J}\cdot\text{cm}^{-2}$ fluency, 6 Hz repetition rate, $19\text{ }\mu\text{m}$ spot-size, and 40 s ablation. Monazite 44069 was employed as primary standard [81, 90]. U–Pb diagrams and final ages were calculated using IsoplotR [85]. Ages and uncertainties are presented with 2σ level of confidence with final ages presented as $x \pm |y|$, with x and $|y|$ representing the age (Ma) the studentized error stated at 95% confidence, respectively.

4. Results

4.1. Macroscopic to Microscopic Structures. The regional shear zones from the southern Ribeira Belt can be divided into five groups based on their orientation and kinematics: NE-trending dextral strike-slip, NE-trending dip-slip, ENE-trending strike-slip, NNE-trending strike-slip shear zones, and NE-trending sinistral strike-slip (Table 1; Figures 2–4). These shear zone groups are classified in types 1 to 5 (Table 1; Figure 3), without chronological implications. The NE-trending strike-slip shear zones are orogen-parallel structures, including the first-order Lancinha and Cubatão shear zones, terrane bounding structures such as the Taxaquara, Serra do Azeite, and Itapirapuã shear zones, and intraterrane structures like the Caucaia, Carumbé, and Putunã shear zones (Figure 1(c)). The other three groups of shear zones are well-developed in the Apiaí Terrane, where the geometrical relationships between the NE-trending dip-slip and ENE-trending dextral strike-slip shear zones develop a dextral S-C'-type shear band macrostructure (Figure 1(c)). Although interconnected, these shear zones present complex structural patterns of interactions and variation in the metamorphic conditions. Type 5 shear zones exclusively occur south of the Lancinha and Cubatão shear zones and will not be considered in this work.

4.1.1. NE-Trending Strike-Slip Shear Zones (Type 1). Type 1 shear zones occur north of the Lancinha and Cubatão shear zones and affect the Apiaí, Embu, and São Rock terranes,

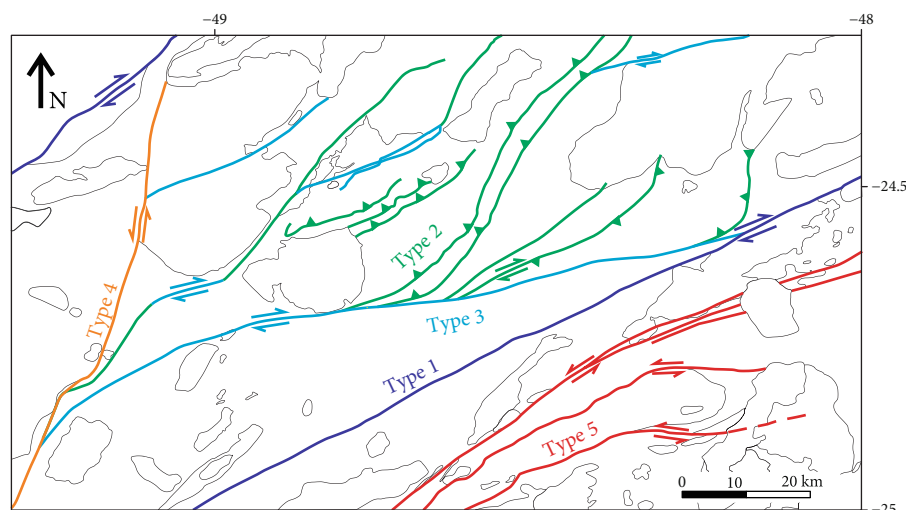


FIGURE 3: Simplified structural map showing the main groups of shear zones. The map uses geographical coordinates in degrees (WGS-84 datum).

and their boundaries. They have a preferential N60°E orientation and cut most other structures including types 2 and 3 shear zones. The Lancinha shear zone has a NW-steep-dipping mylonitic foliation and a SW plunging subhorizontal stretching lineation (Figures 3 and 4). In its northeastern domain, macroscopic (regional pattern of foliation inflection; Figure 2) and microscopic kinematic indicators such as S-C structures, rotated porphyroclasts, and porphyroblasts consistently indicate dextral shear sense (Figures 5(a) and 5(b)). Similarly, dextral shear sense has been reported in the southwestern domain of the Lancinha shear zone on the basis of macroscopic and hand-sample scale structures [91, 92]. Conversely, Conte et al. [26] describe hand-sample and microscopic sinistral indicators in a few outcrops from the central and southwestern domains of the Lancinha shear zone.

Microstructures and grain-scale deformation mechanisms recorded in quartz mylonites suggest variable thermal regimes along the Lancinha shear zone [26]. Deformation in quartz mylonites from the southwestern and central domains of the shear zone was accommodated by dislocation creep, achieving bulging recrystallization and combined subgrain rotation and grain boundary migration recrystallization, respectively [26].

The Itapirapuã shear zone presents an average N40E/subvertical orientation over an along strike distance of ~166 km (Figure 1(c)). It is dominated by a subvertical NE-trending mylonitic foliation with a subhorizontal NE-trending stretching lineation, but its northern termination splays in a set of NNE-trending sinistral and NE-trending and ENE-trending dextral transcurrent shear zones [31]. Domains between shear zones present regional normal-horizontal folds outlined by metalimestone and quartzite bodies [31].

Deformation microstructures in quartz and feldspar aggregates from mylonite rocks from the Itapirapuã shear zone indicate dominance of distinct deformation mechanisms in individual samples of metasedimentary and ortho-

gneiss rocks of contrasting metamorphic grades [31]. Deformation in quartz aggregates from phyllite samples was accommodated by intracrystalline deformation and dissolution-precipitation creep in low-temperature samples, combined subgrain rotation and grain boundary migration recrystallization in medium temperature samples and grain boundary migration in high-temperature paragneiss samples [31]. Feldspar porphyroclasts of all sheared lithotypes present evidence of intracrystalline deformation (undulose extinction, deformation lamellae, deformation twinning, and twin boundary migration recrystallization), with σ -type and δ -type kinematic indicators [31].

Quartz mylonites occurring at northeastern portion of the Lancinha shear zone, at its junction with the Ribeira shear zone, present rare millimeter-sized, moderately elongated ribbon quartz grains with an aspect ratio ranging from 2:1 to 5:1 set in a matrix of coarse-grained recrystallized grains. Ribbon and recrystallized quartz grains show undulose extinction. Recrystallized grains represent ~80% volume of the rock, being very irregular in shape and size (average grain sizes of $139 \pm 52 \mu\text{m}$), commonly presenting lobate boundaries (Figure 5(c)). Quartz-ribbons locally show relatively small subgrain structures developed towards grain boundaries, being commonly associated with polygonal, recrystallized grains of the same grain size, suggesting a subgrain rotation contribution or overprint. New grains formed by bulging recrystallization locally occur (Figure 5(c)).

Mylonitic granites present saussuritized feldspar porphyroclasts in a recrystallized matrix segregated in an anastomosing net of interconnected quartz and biotite-rich domains (Figure 5(d)). Feldspar grains are fragmented to rounded, reach up to 3 mm in size, and present intra- and intergranular microfractures and common undulose extinction (Figure 5(d)). The matrix is dominated by biotite-rich aggregates, forming lepidoblastic shear bands. Quartz aggregates occur in restricted monomineralic lenses in the matrix and present interlobate granoblastic microstructure.

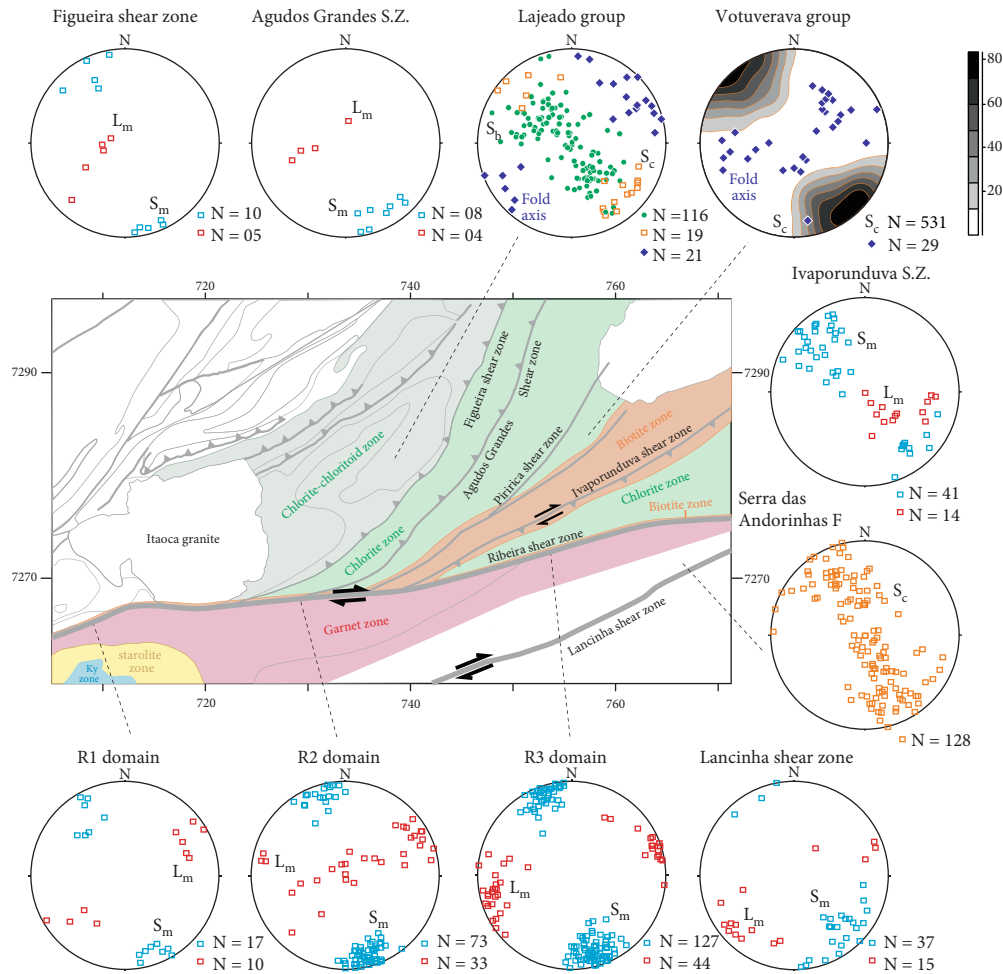


FIGURE 4: Simplified metamorphic-structural map showing the metamorphic zonation of the part of the Apiaí Terrane (after Faleiros et al. [22] and Yogi [58]) and field structural data for the main geological units and shear zones. Structural data: S_m , mylonitic foliation; L_m , stretching lineation; S_b , sedimentary bedding; S_c , continuous cleavage or schistosity. Colored fields in the map represent the metamorphic zones (light green: chlorite-chloritoid zone; green: chlorite zone; orange: biotite zone; red: garnet zone). R1, R2, and R3 represent three domains of the Ribeira shear zone with different orientations. The map uses UTM coordinates in km (WGS-84 datum, zone 22S).

4.1.2. NE-Trending Dip-Slip Shear Zones (Type 2). Type 2 shear zones are essentially intraterrane structures with variable orientation between N10 and 60°E with an average of N35°E. The Figueira, Agudos Grandes, Piririca, Ivaporunduva, and Batal shear zones are the main examples of this group (Figures 3 and 4), which also include third-order thrust faults along the contacts between the formations of the Lajeado Group (Figures 2–4).

Geometrical relationships and orientation patterns suggest that type 2 shear zones are coeval with horizontal-normal folds with NE-trending traces present in the Lajeado and Votuverava groups (Figures 2–4). The Lajeado Group macrostructure consists of large-scale open synclines and anticlines with NE-trending subhorizontal axes and associated NW-steep-dipping axial-plane foliation (Figure 2). This foliation in metapelitic rocks is a continuous cleavage (S_c) defined by oriented sericite, chlorite, and elongated quartz (Figure 6(a)). Chloritoid porphyroblasts are late-kinematic

in relation to the S_c foliation (Figure 6(a)). The metamorphic mineral assemblage indicates lower greenschist facies metamorphic conditions for the Lajeado Group rocks. The Votuverava Group comprises isoclinal folds (Figure 6(b)) with NE-trending axes and axial-plane continuous schistosity (S_c) dipping steeply northwestwards (Figure 4). The S_c schistosity in metapelites to the north of the Ribeira shear zone is primarily defined by sericite, chlorite, biotite, and elongated quartz, which is parallel to subparallel to the sedimentary bedding (Figure 6(b)). Mineral assemblages indicate lower greenschist facies metamorphic conditions varying from chlorite to biotite zones for rocks to the north of the Ribeira shear zone (Figure 4). To the south of the Ribeira shear zone, higher-grade metamorphic zones are represented by garnet, staurolite, and kyanite zones (Figure 4).

The NE-trending dip-slip shear zones and related structures are deflected along the ENE-trending strike-slip shear zones indicating regional-scale dextral kinematics for the

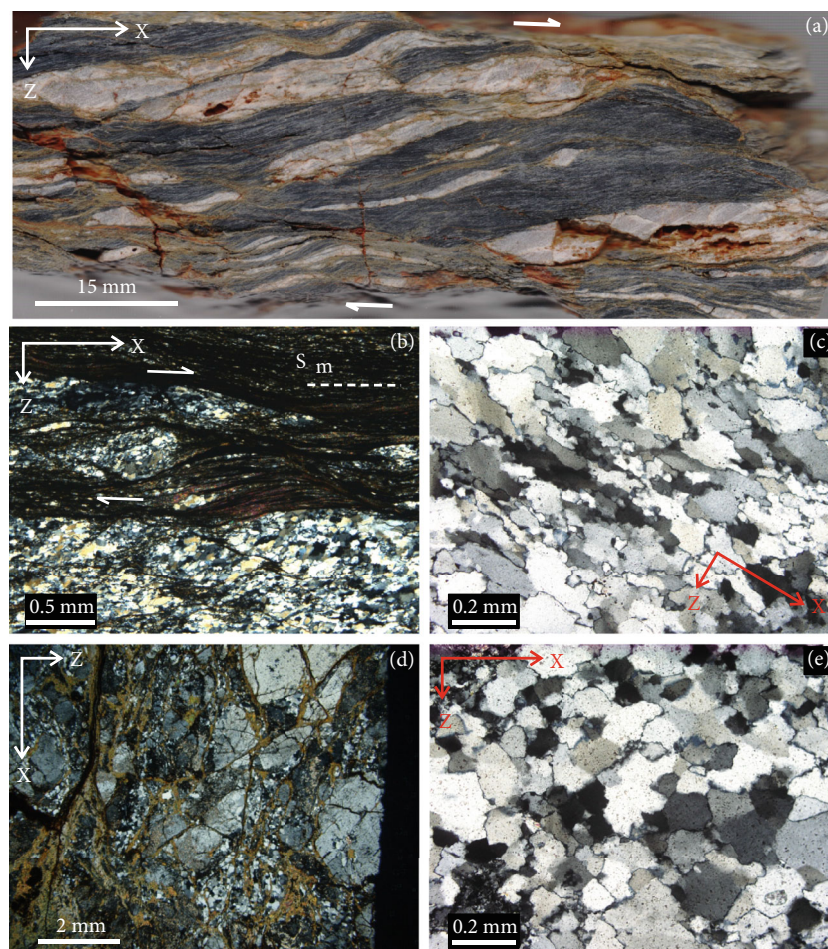


FIGURE 5: Structures and microstructures of rocks from the northeastern portion of the Lancinha shear zone observed on XZ sections of the strain ellipsoid. (a) Dextral S-C structures in a mylonitic biotite schist with strained quartz veins (outcrop M173). (b) Dextral C' -type shear band cleavage and completely recrystallized quartz aggregates in a mylonitic biotite schist (sample M173A). (c) Recrystallized aggregate of quartz with interlobate granoblastic microstructure generated by grain boundary migration in a quartz mylonite (sample F42B). Localized bulges along grain boundaries indicate a bulging recrystallization superposition. (d) Mylonitic granite with fractured feldspar porphyroclasts in an anastomosing network of recrystallized matrix segregated in biotite-rich and quartz-rich domains (sample F46A). (e) Detail of quartz aggregate with interlobate granoblastic microstructure and restricted bulges formed by grain boundary migration and bulging recrystallization, respectively (sample F46A).

latter (Figure 2). This pattern is also observed in the mylonitic foliations of the Figueira and Agudos Grandes shear zones that dip steeply to NW (relicts) and NNW (deflected) as an effect of the interaction between the two groups of shear zones (Figure 4). The stretching lineation is dominant of a high-angle in the dip-slip shear zones, although subhorizontal lineation in zones of interference with strike-slip faults also occurs (Figure 4; Figueira, Agudos Grandes, and Ivaporunduva shear zones).

Field and microscopic S-C structures and rotated porphyroclasts observed in type 2 shear zones indicate reverse movement, with upper block transport to SE (Figure 6(c)). On the other hand, the Ivaporunduva shear zone dips primarily to SE and presents top-to-the-NW shear sense indicators observed on the XZ section of the strain ellipsoid (Figure 6(e)) and dextral shear sense indicators observed on the horizontal YZ section (Figure 6(f)).

Tectonites associated with the NE-trending dip-slip shear zones present the same lower greenschist facies metamorphic conditions of the less deformed host rocks from the Lajeado and Votuverava groups. Sheared metasedimentary rock deformed along the Figueira shear zone presents millimeter-thick layers of quartz-rich cataclasite interlayered with thin sericite-rich shear bands (Figure 6(d)). Cataclasite layers present angular grains of quartz and subordinate feldspars randomly oriented, with a seriate variation of grain sizes. Some larger quartz grains present undulose extinction and recrystallized grains with sizes of 5–10 μm along grain boundaries and forming the matrix. The sericite-rich shear bands present lepidoblastic texture defined oriented sericite, chlorite, and elongated quartz grains (Figure 6(d)).

Quartz mylonites from the Ivaporunduva shear zone present moderately flattened quartz porphyroclasts with irregular undulose extinction and restricted aggregates of

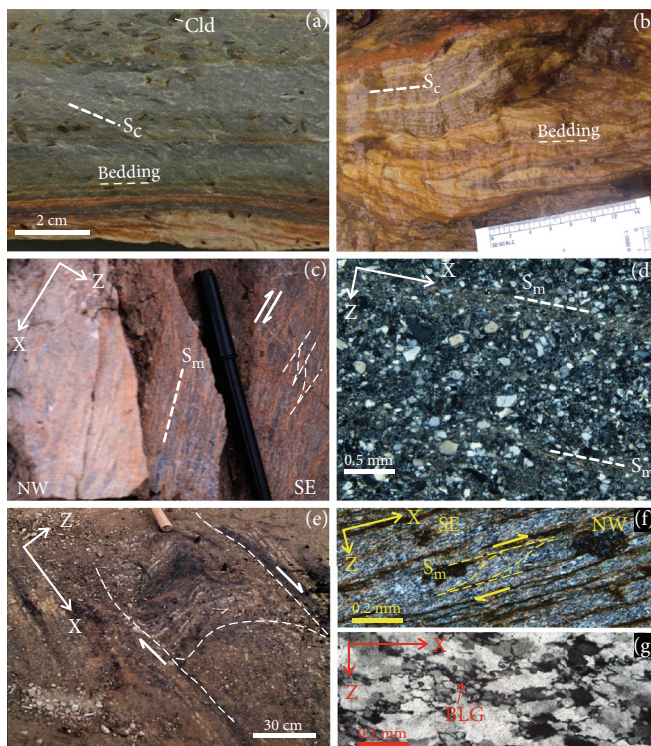


FIGURE 6: (a) Slate from the Lajeado Group showing sedimentary bedding, cross lamination, a continuous cleavage (S_c), and millimetric porphyroblasts of chloritoid (Cld). (b) Isoclinal fold of sedimentary bedding and parallel continuous cleavage (S_c) in a rhythmic metapelite (phyllite) from the Votuverava Group to the north of the Ribeira shear zone. (c) Protomylonitic phyllite from the Figueira shear zone showing a mylonitic foliation (S_m) and top-to-the-SE C' -type shear band cleavage (outcrop F196). (d) Alternating bands of quartz-rich cataclasite and lepidoblastic sericite-rich mylonitic shear bands (S_m) in a protomylonitic phyllitic from the Figueira shear zone (sample F196). (e) Dextral S-C structure in a mylonitic phyllite from the Votuverava Group along the Ivaporunduva shear zone. (f) C-type shear band cleavage indicating top-to-the-NW sense of shear in mylonitic biotite-sericite schist from the Ivaporunduva shear zone (sample SZ85A). (g) Quartz mylonite from the Ivaporunduva shear zone showing elongated quartz porphyroclasts with undulose extinction and aggregates of very fine-grained recrystallized grains along their boundaries, formed by bulging recrystallization (BLG). Images (c) to (g) represent the XZ sections of the strain ellipsoid.

recrystallized grains (5-10 μm) along grain boundaries (Figure 6(g)).

4.1.3. ENE-Trending Strike-Slip Shear Zones (Type 3). The Ribeira shear zone is the main example of the type 3 shear zones, with N80°E mean orientation, subvertical mylonitic foliation, and dominant subhorizontal stretching lineation (R1 and R3 domains, Figures 3, 7(a), and 7(b)). Abundant oblique to down-dip stretching lineations occurs at the interference zone between the Ribeira, Figueira, and Agudos Grandes shear zones (Figure 4).

Type 3 shear zones show macroscopic, mesoscopic, and microscopic dextral kinematic indicators observed in the horizontal plane (XZ section of the strain ellipsoid). The regional inflection of structures around the Ribeira shear zone shows a major dextral horizontal movement (Figures 2–4), with a calculated displacement of ~50 km (see Figure 1(c); [93]). Rotated fragments and boudins and mesoscopic and microscopic S-C structures also indicate a dextral shear sense (Figures 7(b) and 7(c)). The R2 domain of the Ribeira shear zone, where it superposes type 2 shear zone fabrics (Figure 4), is dominated by high-angle stretching lineation (Figure 4), which shows reverse shear sense criteria observed

in vertical YZ planes of both metasedimentary rocks of the Votuverava Group (see Figure 4(d) of Salazar et al. [94]) and granitic rocks from the Itaoca Granite, where the north block ascended in relation to the south block.

The Ribeira shear zone controls the metamorphic zonation of the Apiaí Terrane, limiting a lower greenschist facies domain to the north (chlorite zone rocks), and a middle greenschist to amphibolite facies domain to the south (biotite, garnet, staurolite, and kyanite zone rocks) (Figure 4; [22, 58]). Mylonites along the highest deformation domain of the shear zone interior vary from chlorite to garnet zone conditions southwards, indicating an increase in the deformation temperature [22]. The variation in metamorphic conditions is accompanied by changes in the dynamic recrystallization regimes in quartz mylonites with dominant bulging recrystallization in the chlorite zone mylonites (Figure 7(d)), subgrain rotation in the biotite zone mylonites (Figure 7(e)), and grain boundary migration in the garnet zone mylonites (Figure 7(f)) [22].

4.1.4. NNE-Trending Strike-Slip Shear Zones (Type 4). The Morro Agudo shear zone is the main example of type 4 shear zones, with an approximate N10°E orientation and subvertical

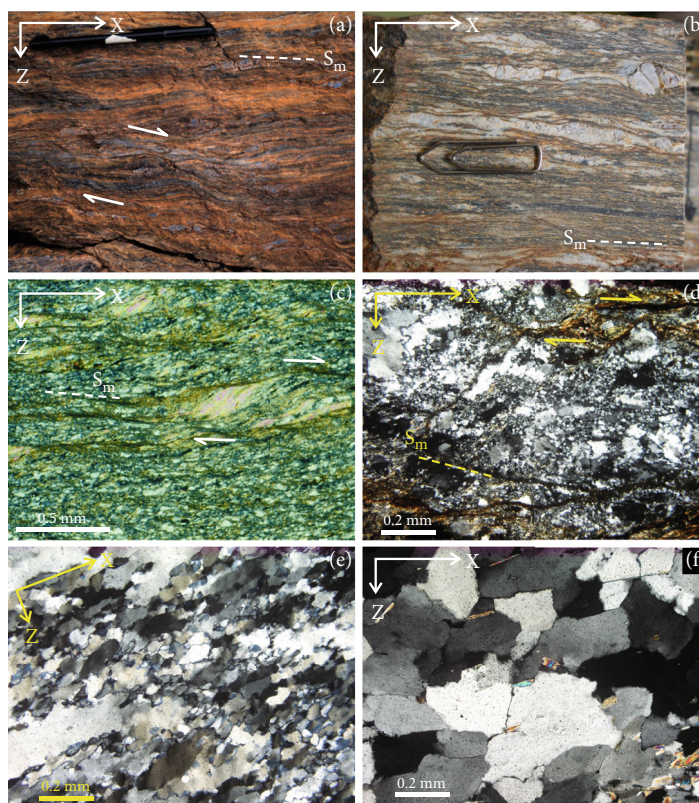


FIGURE 7: Images showing structures and microstructures of mylonitic rocks from the Ribeira shear zone observed on XZ sections of the strain ellipsoid. (a) Dextral $S-C'$ structure in a mylonitic schist. (b) Anastomosing foliation in a mylonitic schist. (c) Dextral C -type shear band cleavage and mica-fish in a mylonitic chlorite-biotite schist from the biotite zone. (d) Bulging recrystallization microstructures in a mylonitic chlorite phyllite from the chlorite zone. (e) Recrystallized matrix of quartz formed by subgrain rotation recrystallization in a quartz mylonite from the biotite zone. (f) Interlobate quartz aggregate formed by grain boundary migration in a quartz mylonite from the garnet zone.

foliation (Figures 2–4). The Morro Agudo shear zone shows regional patterns of foliation deflection, and mesoscale $S-C$ structures and foliation geometry indicative of sinistral shear sense (Figure 8(a)). Related rocks are dominated by breccia and cataclasite, which are well-developed from granitic protoliths of the Três Córregos Suite (Figures 2 and 8(b)–8(d)). The suite is cut by a breccia domain with angular fragments of the host ultracataclasite set in a fluorite-rich matrix (Figure 8(d)).

4.2. Isogon Patterns. The isogon map was constructed using the average orientation of the Ribeira shear zone ($N80^{\circ}E$) as reference (Figure 9). The angle between the major NE-trending structures is up to 60° in domains distant from the Ribeira shear zone and is progressively inflected down to 10° towards its core (Figures 2 and 9). The isogons are disturbed around type 2 shear zones, indicating an obliquity between the associated mylonitic foliation and these shear zones.

There is a strong parallelism between the Ribeira shear zone and the 10° to 25° isogons, primarily in the domain to the north of the shear zone. The 25° isogon remains parallel to the Ribeira shear zone for a long distance, but it is deflected anticlockwise to the NE-trend in the interference zone with subsidiary type 2 shear zones (Figure 9). The isogons show regular ENE-trending orientation in the domain

south of the Ribeira shear zone, maintaining the parallelism with it and the Lancinha shear zone. Nevertheless, an anomalous pattern occurs in the Anta Gorda anticlinorium, where the isogons show a NW-trending orientation (Figure 9).

4.3. Finite Strain Data. Finite strain results for eight samples are presented in Figure 10 with their respective ellipsoid shape classification according to Jelinek [95]. The calculated finite strain ellipsoids show results with low values of \sqrt{F} between 0.9 and 7.5%, indicating good elliptical adjustment and data quality (Table 2).

The new data show calculated NE-trending foliations with poles (represented by the Z -axes) gently plunging to SE and NW, which is very close to those measured in the field (compare Figures 4 and 10). The maximum deformation ratios ($R_{X/Z}$) are dominant of low to intermediate intensity with $R_{X/Z}$ values between 1.3 and 2.8, with some high values of 5.7 and 8.9 (Table 2).

These new data, when combined with published finite strain data from Campanha and Sadowski [93], result in a dataset with 22 quantified samples covering types 2 and 3 shear zones and internal folded domains (Table 2; Figure 11). Samples from the Ribeira shear zone present slightly to strongly oblate-shaped ellipsoids (M215, M183, M206A, M51, and F198; Figures 10 and 11). Calculated X

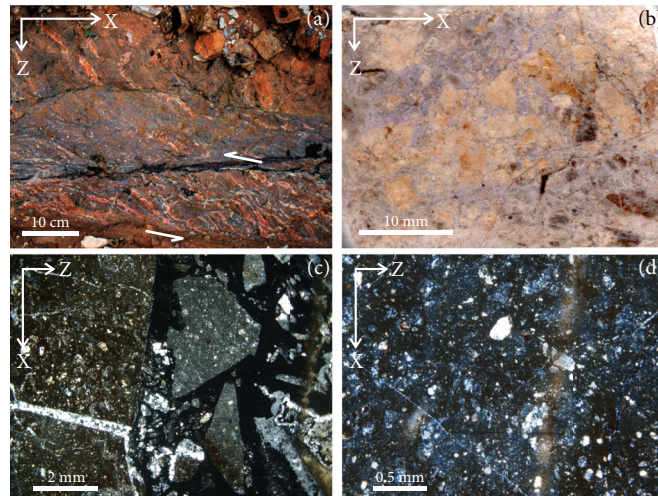


FIGURE 8: Structures and microstructures of cataclastic rocks from the Morro Agudo shear zone observed on XZ sections of the strain ellipsoid. (a) Brecciated protomylonite showing sinistral S-C structures. (b) Brecciated tectonite derived from granite with angular fragments of ultracataclasite in a fluorite-rich matrix (sample F1C). (c) Detail of ultracataclasite cut by a millimeter-thick breccia domain with fluorite-rich matrix (sample F1C). (d) Detail of ultracataclasite composed of rare angular grains of quartz and saussuritized feldspar (up to 0.1 mm in size) in a cryptocrystalline matrix (sample F1C).

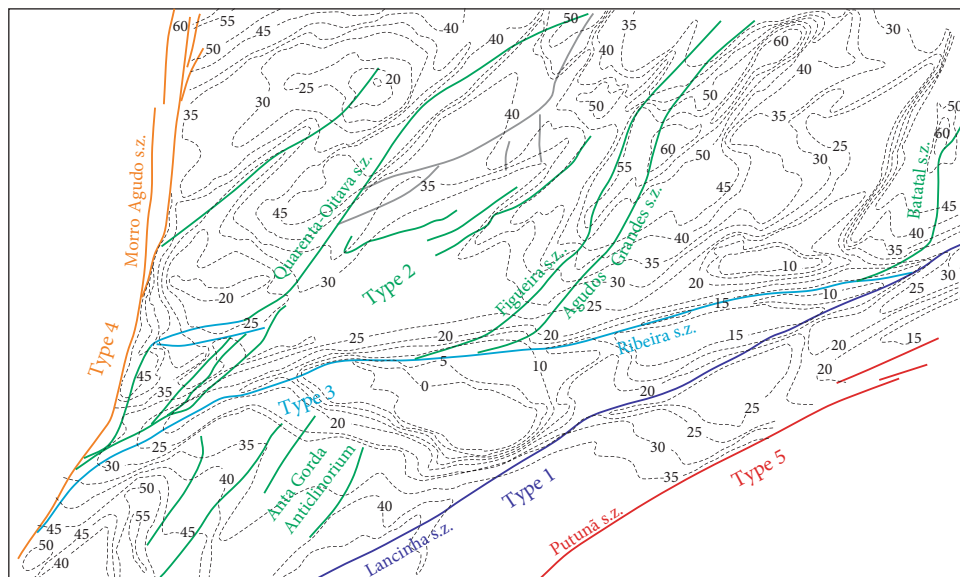


FIGURE 9: Isogon map calculated taking the orientation of the Ribeira shear zone (N80°E) as reference.

-axes (stretching lineation) are subhorizontal, oblique, and down-dip plunges, with a strong correlation with the field structural domain R1 to R3 (Figure 10).

Samples from most of type 2 shear zones have slightly to strongly prolate-shaped ellipsoids and down-dip X-axes (stretching lineations) (Figure 11), corroborating field-based structural data. Samples M193A and M193B (prolate-shaped) and IP538 (oblate-shaped) from the Piririca shear zone have calculated subhorizontal stretching lineations (Figures 10 and 11), indicating strike-slip movement.

Samples obtained from low-grade metasedimentary rocks in the internal domain of the Lajeado Group show

low strain ratios ($1.28 < X/Z < 1.91$), plane strain to prolate-shaped strain geometry, and subhorizontal or down-dip X-axes (Figure 11).

4.4. Kinematic Vorticity

4.4.1. δ/β -Method. Overall, there is a predominance of cross-girdle quartz CPO with vorticity angle (β) from 15° to 25° in the Ribeira shear zone samples (Figure 12), with one sample being mostly symmetrical with β of ~0° (M160) and one mostly monoclinic (single girdle) with β of ~18°. Samples with clear orthorhombic fabric define a $W^{\delta/\beta}_m$ interval

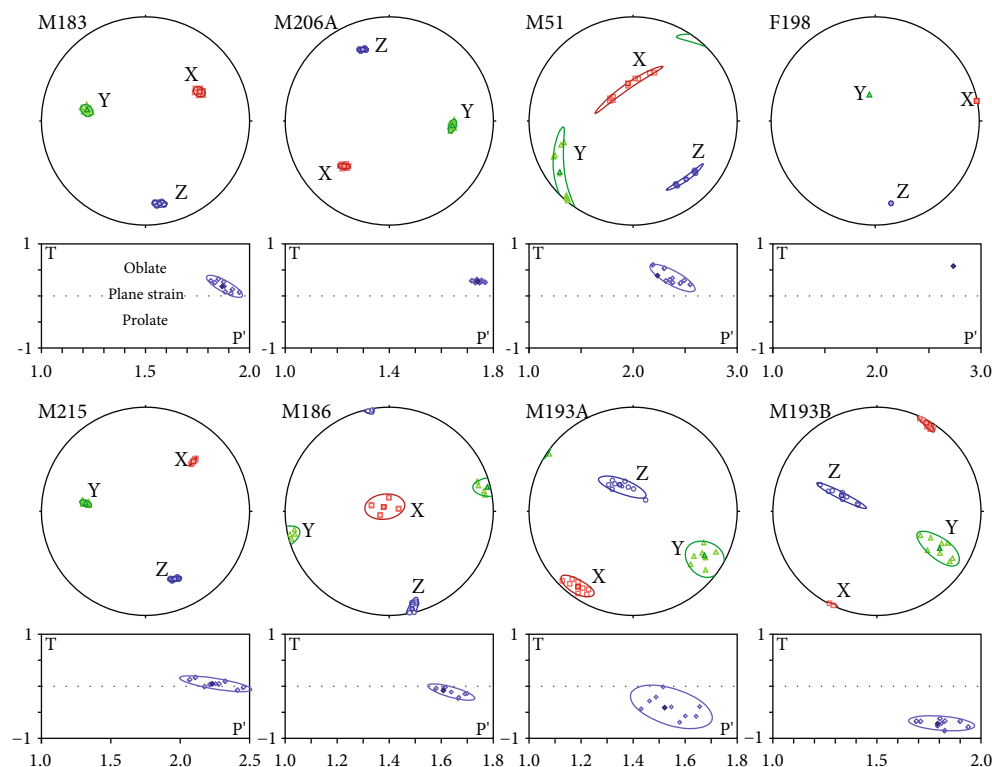


FIGURE 10: Three-dimensional finite strain data from the Ribeira shear zone and associated structures with ellipsoid shape characterized by anisotropy degree (P') and shape parameter (T) of Jelinek [95].

spanning 0.41–67, whereas two samples (F34D and M214C) with cross-girdles have $W^{\delta/\beta}_m$ spanning 0.93–99 due to the higher δ angle (i.e., the maximum angle between quartz oblique fabric and main foliation defined in thin section) (Table 3). Two samples with monoclinic fabric (M161H and M23) have high $W^{\delta/\beta}_m$ yielding 0.93 and 0.99 with clear dominance of simple shear contribution as expected (e.g., Hunter et al., 2018).

4.4.2. Rigid Porphyroclast Method. Mylonite samples related to the Ribeira shear zone (type 3) generally define similar W^{RP}_m values (Figure 13; Table 3). For instance, five out of seven samples are within a W^{RP}_m range of 0.53–0.79, indicating ~65–40% of pure shear contribution. The remaining two samples (M215 and M193A) have comparatively higher W^{RP}_m of ~0.76–0.88 and ~0.82–0.89, suggesting a greater contribution of simple shear.

Vorticity results from types 1, 2, and 4 shear zones also define a similar W^{RP}_m range spanning 0.57–0.80 (Figure 14). These mean vorticity numbers are very similar to those from the majority samples of the Ribeira shear zone, indicating ~65–40% of pure shear contribution.

4.5. U–Pb Geochronology and Trace Element Concentrations. To better constrain metamorphic events and the timing of shearing of the southern Ribeira Belt, we applied U–Pb isotope systematics to minerals from mylonitic rocks of varied metamorphic grades from the Itapirapuã and Ribeira shear zones (types 1 and 3 shear zones, respectively). Samples P33 (mylonitic paragneiss) and CA29 (mylonitic phyllite)

from the Itapirapuã shear zone (Figure 1(c)) display contrasting metamorphic conditions (Table 4) and were chosen to investigate if there is more than one deformational/metamorphic episode recorded along with this type 1 structure. Samples M214C (mylonitic garnet-biotite schist) and DC59A from the Ribeira shear zone (type 3 structure) were collected along its main segment and at the interference domain with the Lancinha shear zone (type 2 structure), respectively (Figure 2). We analyzed monazite and xenotime grains from sample P33, titanite from sample CA29, monazite from sample M214C, and zircon from sample DC59A. The geochronological results are summarized in Table 4, and the complete dataset is presented in supplementary material (available here).

Sample P33 is a mylonitic paragneiss with millimetric granitic lenses (leucosome) molded by schistose domains composed of biotite, quartz, muscovite, fibrolitic sillimanite, and minor ilmenite. Monazite grains are generally smaller than 50–60 μm , often displaying fractures and sector zoning in backscatter electron images (Figure 15(a), inset). A total of 38 monazite U–Pb–REE data were collected from sample P33, from which 37 pass the filtering criteria of maximum $\pm 10\%$ discordance. Monazite REE-chondrite normalized profiles define a coherent chemical pattern with La depletion, dominance of LREE, and negative Eu anomalies with Eu/Eu^* spanning 0.18–0.33 (Figure 15(b)). Most of these monazite grains ($N = 34$) yield a concordia age of 675 ± 7 Ma (MSWD = 1.0, Figure 15(c)), with few U–Pb data from darker domains of the sector zoning (see Figure 15(a), inset) defining an average $^{206}\text{Pb}/^{238}\text{U}$ age of 825 ± 24 Ma

TABLE 2: Finite strain results for samples of dip-slip and strike-slip shear zones and internal domains of the Apiaí Terrane. Shear zone and Group are abbreviated to “s.z.” and “G.,” respectively.

| Sample | Shear zone or unit | XY plane | Axes values | | | Axes orientations | | | X/Z | X/Y | Y/Z | K | (F) ^{1/2} (%) |
|-----------------------------------|---------------------|----------|-------------|------|------|-------------------|--------|--------|------|------|------|------|------------------------|
| | | | X | Y | Z | X | Y | Z | | | | | |
| <i>This work</i> | | | | | | | | | | | | | |
| M183 | Ribeira s.z. | 260/69 | 0.84 | 1.39 | 2.87 | 062/40 | 280/42 | 170/21 | 1.85 | 1.29 | 1.44 | 0.65 | 6.3 |
| M206 | Ribeira s.z. | 069/62 | 0.59 | 0.87 | 1.75 | 225/38 | 095/39 | 339/27 | 1.72 | 1.22 | 1.42 | 0.52 | 4.3 |
| M51 | Ribeira s.z. | 227/65 | 0.61 | 0.98 | 2.88 | 352/60 | 235/15 | 137/25 | 2.17 | 1.27 | 1.71 | 0.37 | 7.5 |
| F198 | Ribeira s.z. | 259/69 | 0.14 | 0.15 | 1.13 | 076/07 | 328/68 | 168/20 | 2.81 | 1.03 | 2.73 | 0.02 | 0.9 |
| M215 | Ribeira s.z. | 246/60 | 0.30 | 0.64 | 1.46 | 044/34 | 277/41 | 156/30 | 2.21 | 1.46 | 1.51 | 0.89 | 3.8 |
| M186 | Ivaporunduva s.z. | 257/85 | 0.97 | 1.62 | 2.50 | 308/84 | 076/03 | 167/04 | 1.60 | 1.29 | 1.24 | 1.20 | 4.5 |
| M193A | Piririca s.z. | 063/23 | 0.63 | 1.12 | 1.43 | 216/11 | 122/20 | 333/66 | 1.50 | 1.33 | 1.13 | 2.60 | 4.6 |
| M193B | Piririca s.z. | 024/30 | 0.46 | 1.15 | 1.34 | 029/03 | 121/30 | 294/59 | 1.71 | 1.58 | 1.08 | 7.41 | 4.9 |
| <i>Campanha and Sadowski [93]</i> | | | | | | | | | | | | | |
| AP001 | Lajeado G. | 179/71 | 1.46 | 1.00 | 0.64 | 258/32 | 114/52 | 359/19 | 2.30 | 1.46 | 1.56 | 0.81 | — |
| AP065 | Dip-slip s.z. | 001/30 | 1.31 | 1.00 | 0.75 | 012/30 | 279/02 | 181/60 | 1.74 | 1.31 | 1.33 | 0.93 | — |
| AP117 | Lajeado G. | 300/47 | 1.32 | 1.00 | 0.83 | 023/08 | 286/46 | 120/43 | 1.59 | 1.32 | 1.20 | 1.62 | — |
| IP060 | Lajeado G. | 307/70 | 1.29 | 1.00 | 0.78 | 310/70 | 217/03 | 127/20 | 1.65 | 1.29 | 1.28 | 1.03 | — |
| IP064 | Lajeado G. | 312/87 | 1.46 | 1.00 | 0.88 | 222/05 | 015/84 | 132/03 | 1.67 | 1.46 | 1.14 | 3.32 | — |
| IP071 | Lajeado G. | 250/81 | 1.13 | 1.00 | 0.88 | 180/62 | 336/26 | 070/09 | 1.28 | 1.13 | 1.14 | 1.02 | — |
| IP253 | Dip-slip s.z. | 312/22 | 1.12 | 1.00 | 0.83 | 284/20 | 017/10 | 132/68 | 1.35 | 1.12 | 1.20 | 0.62 | — |
| IP538 | Piririca s.z. | 311/80 | 2.41 | 1.00 | 0.27 | 224/20 | 020/68 | 131/10 | 8.93 | 2.41 | 3.70 | 0.52 | — |
| IP808 | Lajeado G. | 300/82 | 1.37 | 1.00 | 0.72 | 030/12 | 240/75 | 120/08 | 1.91 | 1.37 | 1.39 | 0.95 | — |
| IP928 | Lajeado G. | 226/32 | 1.20 | 1.00 | 0.92 | 179/27 | 280/20 | 046/58 | 1.31 | 1.20 | 1.09 | 2.24 | — |
| IP931 | Dip-slip s.z. | 349/63 | 1.35 | 1.00 | 0.93 | 042/50 | 275/28 | 169/27 | 1.45 | 1.35 | 1.08 | 5.07 | — |
| IP939 | Agudos Grandes s.z. | 342/88 | 3.99 | 1.00 | 0.69 | 025/72 | 255/12 | 162/02 | 5.74 | 3.99 | 1.45 | 6.78 | — |
| ME004 | Lajeado G. | 345/83 | 1.32 | 1.00 | 0.70 | 068/50 | 262/47 | 165/07 | 1.87 | 1.32 | 1.43 | 0.75 | — |
| P26 | Figueira s.z. | 294/64 | 1.82 | 1.00 | 0.65 | 348/50 | 218/28 | 114/26 | 2.78 | 1.82 | 1.54 | 1.55 | — |

(MSWD = 0.6, $N = 3$) (Figure 15(c), inset). Xenotime is rare in sample P33, generally presenting anhedral shapes, fractures, and sector zoning in backscatter electron images (Figure 15(d)). The dark zones generally present higher Mg and La, but it is not consistent for all spots, possibly due to mixing with other zones. The xenotime REE-chondrite normalize profiles are similar to all analyzed spots, with negative Eu anomaly (Eu/Eu* ranging from 0.30 to 0.38) and strong HREE enrichment with (Gd/Yb)_N spanning 0.04–0.08 (Figure 15(e)). Most of the xenotime U–Pb data ($N = 8$), generally related to brighter zones, yield a concordia age of 829 ± 18 Ma (MSWD = 0.4, Figure 15(f)). This age is very similar to that recorded by a few of the sector zones in monazite grains. However, three xenotime U–Pb data related to darker sector zones yield an average $^{206}\text{Pb}/^{238}\text{U}$ age of 721 ± 25 Ma (Figure 15(f), inset).

Sample CA29 is a greenish grey mylonitic phyllite composed of quartz, phengite, biotite, chlorite, titanite, ilmenite, and minor rutile and epidote. The sample presents alternating quartz-rich and mica-chlorite-rich lenses parallel to an anastomosing mylonitic foliation (S_m) defined by preferred orientation of micas and chlorite. Porphyroblastic titanite grains are euhedral to subhedral presenting asymmetric strain shadows indicating dextral shear sense (Figure 16(a),

inset). We collected a total of 42 titanite U–Pb–REE data from sample CA29, from which 13 data are spurious and six are over discordant (greater than 2σ) in relation to the main trend defined in the Tera-Wasserburg diagram. The remaining titanite grains ($N = 23$) have concave REE-chondrite normalized profiles with dominance of MREE (Figure 16(a)) and can be chemically classified into two groups based on the (La/Sm)_N and (Gd/Yb)_N ratios and the MREE content. One group (Figure 16(a), green lines) has the higher MREE content between 326.6 and 926.6 ppm and steeper LREE and HREE trends with (La/Sm)_N and (Gd/Yb)_N spanning 0.09–0.17 and 3.08–5.82, respectively. The other group (Figure 16(a), red lines) has comparatively lower MREE content between 188.9 and 370.8 ppm and shallower LREE and HREE trends with (La/Sm)_N and (Gd/Yb)_N spanning 0.16–0.37 and 1.90–4.17, respectively. Despite being chemically distinct, these titanite grains define a single inverse isochron in the Tera-Wasserburg diagram yielding a lower intercept age of 896 ± 39 Ma (MSWD = 1.8, Figure 16(b)) with an initial $^{207}\text{Pb}/^{206}\text{Pb}$ ratio of 0.902 calculated with Stacey and Kramers [88].

Sample M214C is a mylonitic schist composed of garnet and biotite porphyroblasts in a matrix segregated in quartz-

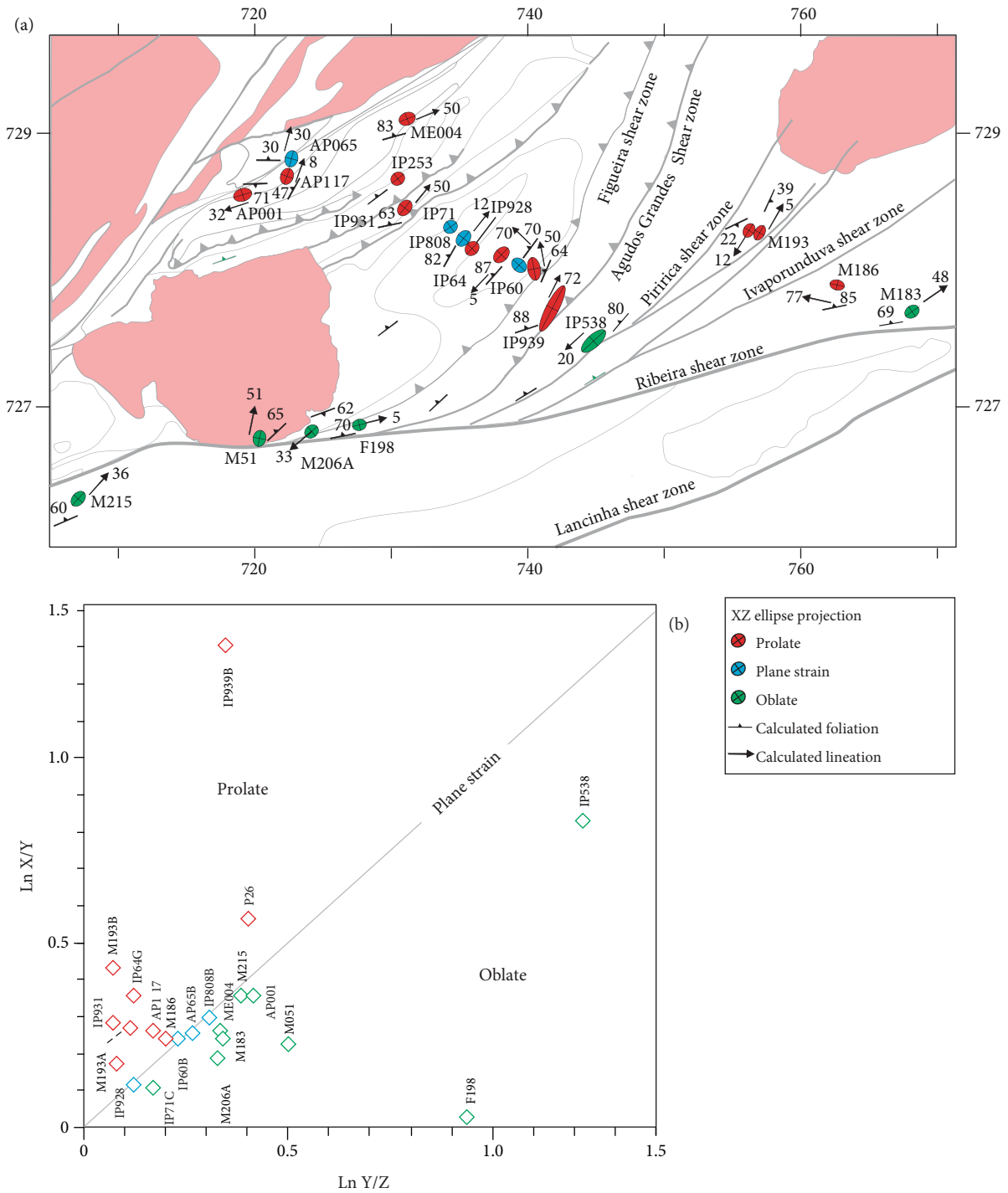


FIGURE 11: (a) Geographic distribution of different types of shape ellipsoids in relation to each structure; (b) Flinn diagram with new and published finite strain data from the southern Ribeira Belt (data compiled from Campanha and Sadowski [93]).

rich layers with interlobate granoblastic microstructure and lepidoblastic biotite-muscovite-rich layers. We collected a total of 19 monazite U–Pb data from sample M214C, of which 13 pass the filtering criteria of maximum $\pm 10\%$ discordance. In short, these monazite grains yield a concordia age of 579 ± 3 Ma (MSWD = 1.9) and a statistically sound average $^{206}\text{Pb}/^{238}\text{U}$ age of 580 ± 4 Ma (MSWD = 1.2, Figure 16(c)).

Sample DC59A is a fine-grained mylonite composed of quartz (95 vol. %), muscovite, and opaque oxide minerals. Quartz grains are elongated, defining the lineation and have irregular, lobate to serrated boundaries. Recrystallized grains define an oblique foliation indicating dextral sense of shear, and the microstructures are compatible with a recrystallization mechanism dominated by grain boundary migration. Zircon grains from sample DC59A have dark grey internal structures

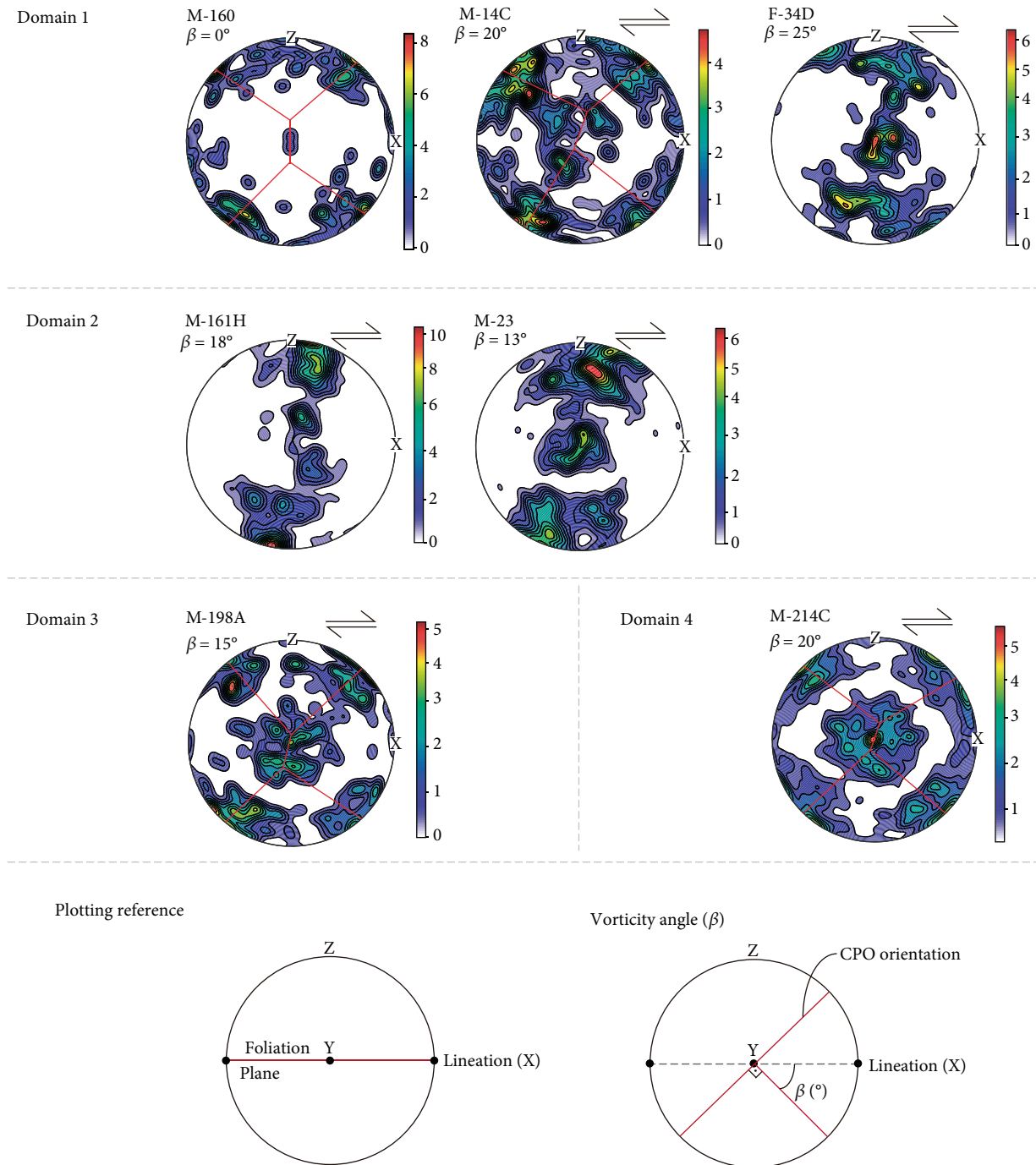


FIGURE 12: Quartz [c]-axis fabric from mylonites associate with the Ribeira shear zone; lower hemisphere equal area projections, foliation oriented left-right and vertical with horizontal stretching lineation (X-direction). Sample number and vorticity angle (β) are indicated in the top right of each plot.

in the cathodoluminescence images (Figure 16(d)), varying from sector to oscillatory zoning. From the 47 zircon U–Pb data collected, a total of 31 data pass the filtering criteria of maximum $\pm 10\%$ discordance. A subset of 19 zircon data with predominant Th/U around 0.1 defines a discordia trend in the Wetherill diagram yielding an upper intercept age of 827 ± 14 Ma (MSWD = 1.2) with lower intercept anchored to zero (Figure 16(d)).

5. Discussion

5.1. Thermal Regimes of Shear Zones from the Ribeira Belt. Microstructures and inferred deformation mechanisms recorded in shear zone-related rocks from the Ribeira Belt indicate that individual shear zones operated across a range of crustal levels. A transitional northeastward increase in metamorphic conditions from lower greenschist (Lancinha

TABLE 3: Vorticity results from rigid porphyroclast and δ/β -methods for samples from types 1 to 4 shear zones.

| Sample | Shear zone | Rigid porphyroclast method | | | | δ/β -method | | | | |
|--------|-------------|----------------------------|--------------|--------------|--------------|------------------------|-------------|----------------------|-------------------|----------------|
| | | R_c min | R_c max | W_m min | W_m max | δ (°) | β (°) | $W^{\delta/\beta}_m$ | Quartz CPO fabric | Pure shear (%) |
| M160 | Ribeira | — | — | — | — | 1.2 | 0 | 0.41 | Crossed girdle | 72 |
| M14C | Ribeira | — | — | — | — | 1.3 | 20 | 0.67 | Crossed girdle | 53 |
| F34D | Ribeira | — | — | — | — | 9.3 | 25 | 0.93 | Single girdle | 24 |
| M161H | Ribeira | — | — | — | — | 16.5 | 18 | 0.93 | Single girdle | 24 |
| M23 | Ribeira | — | — | — | — | 29.9 | 13 | 0.99 | Single girdle | 09 |
| M198A | Ribeira | — | — | — | — | 2.5 | 15 | 0.57 | Crossed girdle | 61 |
| M214C | Ribeira | — | — | — | — | 23 | 20 | 0.99 | Crossed girdle | 09 |
| M206 | Ribeira | 2.2 | 2.8 | 0.66 | 0.77 | — | — | — | — | 54-44 |
| M51 | Ribeira | 2.3 | 2.9 | 0.68 | 0.79 | — | — | — | — | 52-42 |
| F198 | Ribeira | 1.8 | 2.3 | 0.53 | 0.68 | — | — | — | — | 64-52 |
| M215 | Ribeira | 2.7 | 3.7 | 0.76 | 0.86 | — | — | — | — | 45-34 |
| F46A | Lancinha | 1.9 | 2.5 | 0.57 | 0.72 | — | — | — | — | 61-49 |
| F48 | Lancinha | 2.0 | 2.7 | 0.60 | 0.76 | — | — | — | — | 58-45 |
| F196 | Figueira | 2.0 | 3.0 | 0.60 | 0.80 | — | — | — | — | 58-41 |
| F01E | Morro Agudo | 2.0 | 2.7 | 0.60 | 0.76 | — | — | — | — | 58-45 |

segment) to granulite facies metamorphic conditions (Além Paraíba-Pádua segment) is recorded in mylonitic rocks from the first-order NE-trending dextral strike-slip structures. The variation in metamorphic grade is accompanied by changes in recrystallization mechanisms of quartz and feldspar aggregates ([15, 24, 26, 35, 37, 40], this work). Deformation in quartz aggregates was accommodated by dislocation creep achieving bulging recrystallization (300–400°C) and combined subgrain rotation and grain boundary migration (~450–500°C) (Figures 5(b)–5(e)) in the southwest and northeast portions of the Lancinha shear zone, respectively ([26], this work). However, feldspar aggregates were deformed by cataclastic flow (Figure 5(d)) or were replaced by chlorite-epidote-sericite-biotite hydrothermal products. Deformation in quartz aggregates along the Cubatão segment was recrystallized by combined subgrain rotation and grain boundary migration and feldspar aggregates by dissolution-precipitation creep at deformation conditions of 460–520°C and 4.5–9.5 kbar [37]. Quartz aggregates along the Além Paraíba-Pádua segment were deformed under high-temperature conditions achieving pervasive grain boundary migration recrystallization while feldspar aggregates underwent grain size reduction by dynamic recrystallization at thermal conditions from $610 \pm 20^\circ\text{C}$ to $740 \pm 20^\circ\text{C}$ [24].

Quartz aggregate microstructures present in samples from the Figueira and Ivaporunduva shear zones, representative of NE-trending dip-slip (type 2) structures, indicate dominant bulging recrystallization (Figures 6(d) and 6(f)), generally compatible with deformational conditions of ~300–400°C [96, 97]. This inferred thermal regime is corroborated by syn-kinematic metamorphic mineral assemblages of sheared metasedimentary rocks, primarily composed of sericite-quartz-chlorite (Figueira shear zone) and sericite-quartz-chlorite-biotite (Ivaporunduva shear

zone), which are the same assemblages present in the less deformed host rocks affected by regional metamorphism (Figure 4).

Available geothermobarometric results from the Ribeira shear zone, the main example of ENE-trending dextral strike-slip (type 3) shear zones, indicate deformational conditions ranging from ~300°C (chlorite zone) in the northern domain to ~630°C and 5–7 kbar (garnet zone) in the southern domain (Figure 4; [22]). The variation in metamorphic conditions was accompanied by changes in the dominant recrystallization mechanisms of quartz aggregates along the mylonite zone: bulging recrystallization (Figure 7(d); chlorite zone, 300–410°C), subgrain rotation recrystallization (Figure 7(e); biotite zone, 410–520°C), and grain boundary migration recrystallization (Figure 7(f); garnet zone, >520°C) [22]. The available data indicate that the main deformational episode along the Ribeira shear zone was coeval with the regional metamorphism recorded in less deformed host rocks (Figure 4). The higher metamorphic grade in the domain south of the shear zone is a result of a subordinate component of vertical displacement associated with a major horizontal displacement of 50 km along the shear zone [22].

Sheared granitic rocks along the Morro Agudo shear zone, the main example of NNE-trending sinistral strike-slip (type 4) shear zones, are dominated by brittle products (breccia, cataclasite, and ultracataclasite) with quartz and feldspar deformed by cataclastic flow (Figures 8(a)–8(d)), suggesting temperatures below ~250–280°C (e.g., [96–98]). This thermal condition is recorded in Ediacaran granitic rocks (Figure 2) and contrasts with that inferred for a hosting mylonitic paragneiss along the Itapirapuã shear zone (sample P33, 680–690°C [31]; Table 4). These contrasting metamorphic conditions suggest the existence of deformation episodes of distinct ages (see Section 5.3).

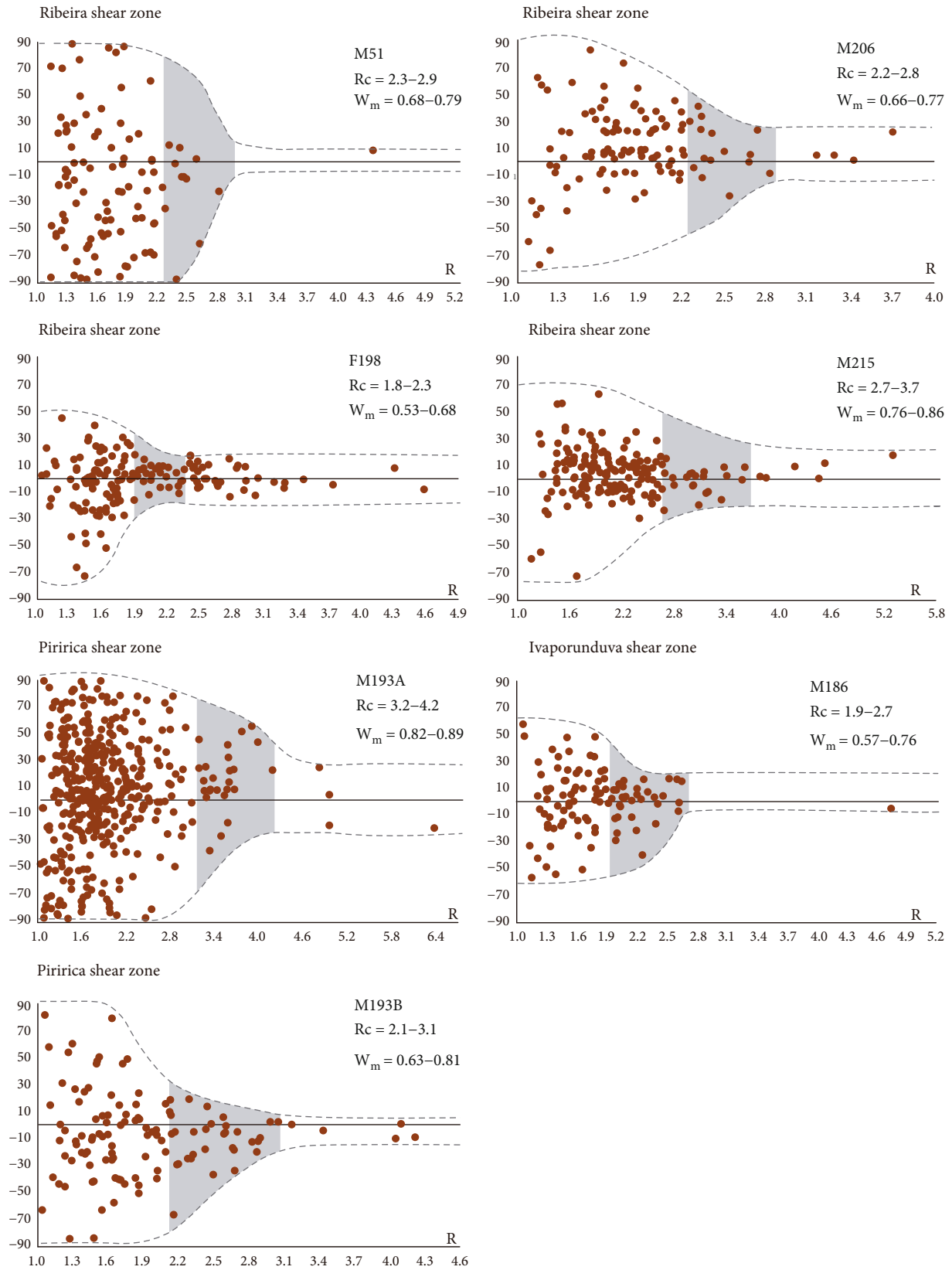


FIGURE 13: Wallis' plots [72] of feldspar porphyroclasts from mylonite related to the Ribeira shear zone and associated structures. The grey field defines a minimum and maximum critical shape ratio (R_c) and its corresponding vorticity number from the rigid porphyroclasts method (W_m^{RP}) for each sample, as indicated in the figure.

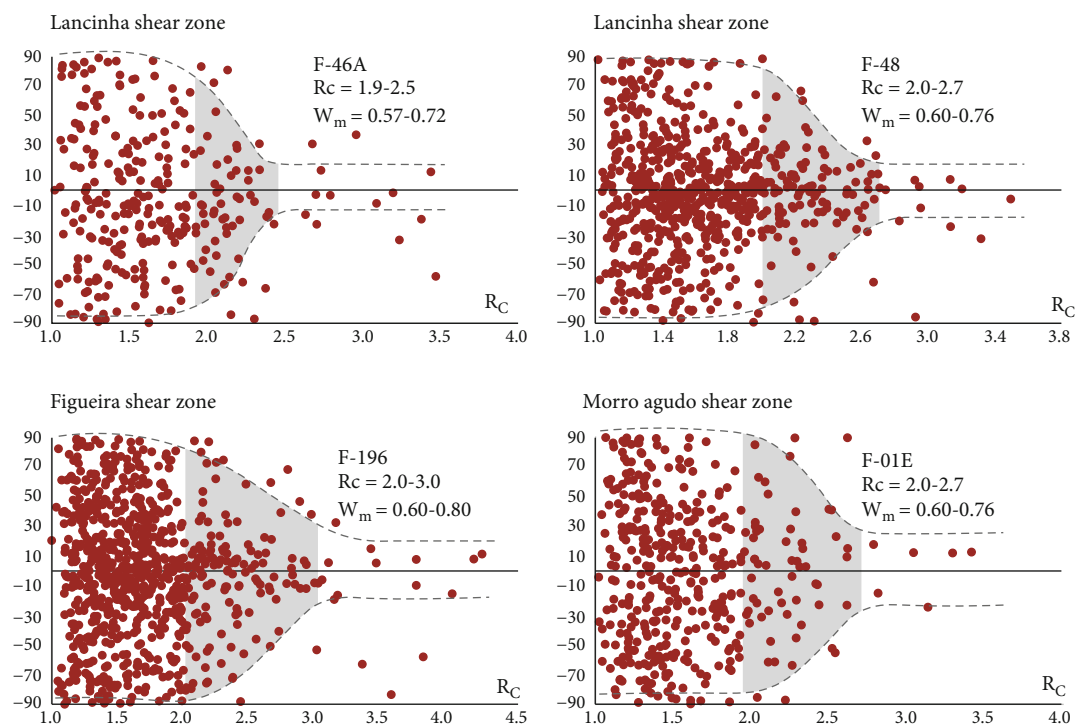


FIGURE 14: Wallis' plots [72] of feldspar porphyroclasts from mylonite-related shear zones from the southern Ribeira Belt (Lancinha, Figueira, and Morro Agudo shear zones). The grey field defines a minimum and maximum critical shape ratio (R_c) and its corresponding vorticity number from the rigid porphyroclasts method (W_m^{RP}) for each sample as indicated in the figure.

In summary, available microstructural and metamorphic data from individual shear zones of the southern Ribeira Belt indicate distinct thermal conditions from subgreenschist to amphibolite facies conditions (<250–280 to ~630°C), with a general correlation with the regional metamorphic conditions recorded in less deformed host rocks.

5.2. Deformational Regimes. At least two endmember models can explain the regional shear zone and tectonic pattern present in the Ribeira Belt: (a) the fabrics are formed during at least two separate tectonic events; (b) the fabrics are the result of a single (progressive) deformation event and are related as S and C fabrics.

At a regional scale, the geometrical relationships between the main groups of shear zones from the southern Ribeira Belt approximate a dextral C' -type shear band macroscopic structure with the C' direction (type 3 dextral ENE-trending strike-slip zones) inclined ~30° relative to the main shear direction (type 1 orogen-parallel NE-trending strike-slip zones) that is subparallel to the S direction (type 2 NE-trending dip-slip zones) (Figure 1(c)). The Lancinha shear zone, the main example of type 1 fabric, would accommodate movements controlled by an ancient plate boundary. At first glance, this bulk kinematics suggests an overall dextral transpressional setting [26, 99], which is corroborated by available finite strain and kinematic vorticity data from individual shear zones [15, 25, 31]. However, some geometrical relationships between the groups of shear zones deviate from theoretical predictions.

In a heterogeneous simple shear model, the angle between the shear direction and the outermost foliation is 45°, which decreases towards the inner domain of the shear zone [1]. In transpressional models, this angle is always lower than 45°, while higher angles are predicted for transtensional zones (e.g., [61, 62, 100–103]). For the Ribeira Belt, the angle between type 3 shear zones (apparent C' direction) and type 2 shear zones (apparent S direction) reaches 60–65° in the outermost portion of the Ribeira shear zone (Figures 2 and 9) deviating from all transpressional model predictions. Transtensional deformation also does not fit the observed geometry, as this model predicts exclusively horizontal stretching lineation and a transition from vertical (simple shear-dominated) to horizontal (pure shear-dominated) mylonitic foliations [61, 62, 100–103] and type 2 zones present subvertical foliation, down-dip stretching lineation, and reverse sense of shear (Figure 4).

Considering these points, the only possible explanation is that type 2 shear zones represent a former tectonic fabric deformed and rotated by the NE and ENE dextral (types 1 and 3) shear zones. This is, for example, the model adopted by Campanha and Sadowski [93] to quantify the shear deformation and the slip along the Ribeira shear zone. Regional and local geological evidence also corroborates this alternative model. The NE and ENE dextral (types 1 and 3) shear zones cut and deform the extensive late Cryogenian to Ediacaran arc-related and postorogenic granites of the Ribeira Belt, but the opposite occurs with the NE-trending dip-slip (type 2) zones, which are interrupted by the granite bodies. Type 2 shear zones in other areas of the Ribeira Belt

TABLE 4: Summary of new geochronological data.

| Sample | Lithotype | Shear zone | Mineral assemblage/deformation mechanism | Isotopic system/phase | P-T conditions | Age (Ma) |
|--------|---------------------------------|----------------------------------------------------|------------------------------------------------|----------------------------|------------------------------------|------------------------------------------------------------------------|
| CA29 | Mylonitic phyllite | Itapirapuá (type 1) | Bt+Chl+Phen+Qz/dissolution-precipitation creep | U-Pb titanite | 490–510°C and 11–12.5 kbar [31] | 896 ± 39 |
| P33 | Mylonitic paragneiss | Itapirapuá (type 1) | Qz+Kfs+Pl+Ms+Bt+Sil/GBM in Qz | U-Pb monazite and xenotime | 680–690°C and 5–6 kbar [31] | 829 ± 18 (Xtm) 721 ± 25 (Xtm) 825 ± 24 Ma (Mnz) 675 ± 7 (Mnz) |
| M214C | Mylonitic garnet-biotite schist | Ribeira (type 3) | Grt+Bt+Ms+Pl+Qz+Ilm/GBM in Qz | U-Pb monazite | 633 ± 27°C and 6.3 ± 1.1 kbar [22] | 580 ± 4 |
| DC59A | Mylonitic quartzite | Ribeira-Lancinha interference zone (type 1-type 3) | Qz+Ms+Opq/GBM in Qz | U-Pb zircon | >500°C [22] | 827 ± 14 |

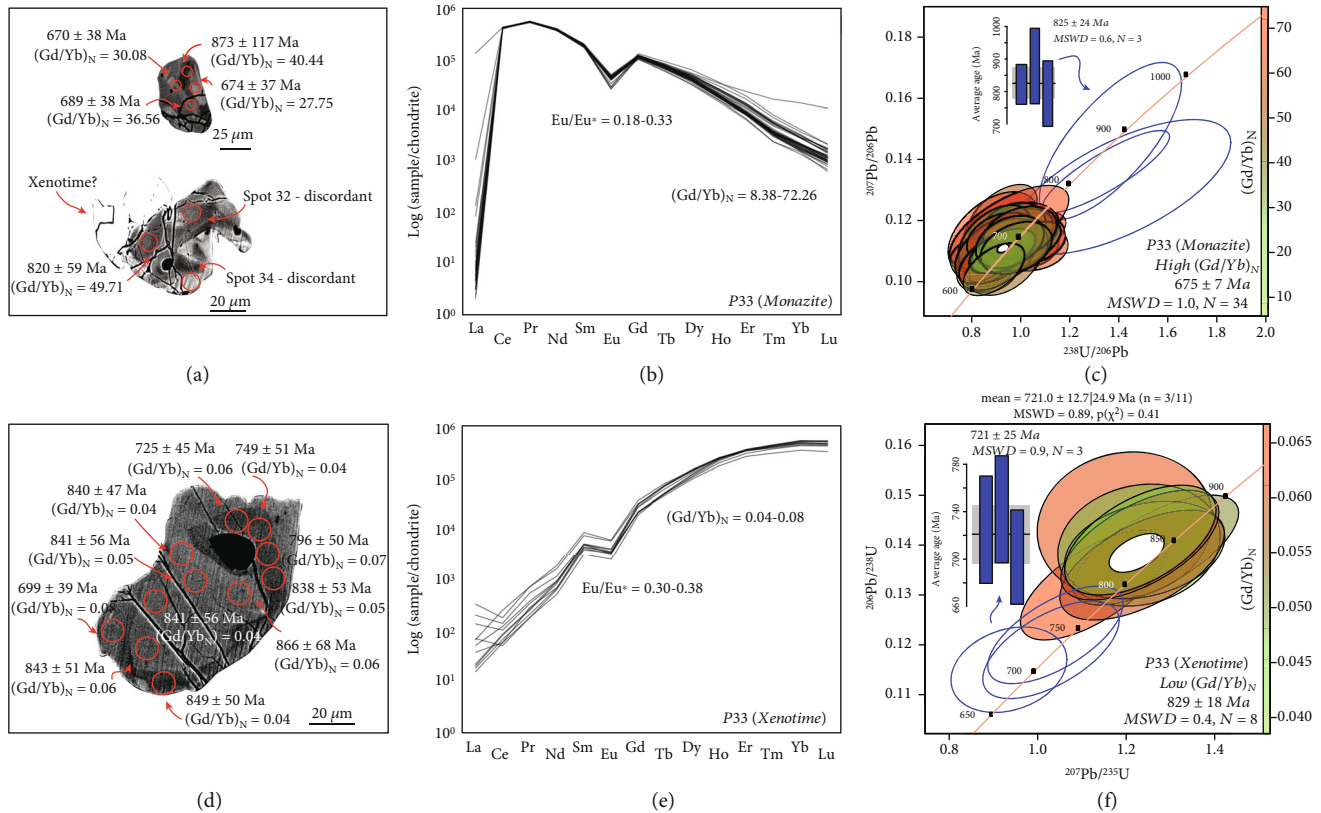


FIGURE 15: Geochronological data from sample P33 associated with the Itapirapuá shear zone. (a) backscatter electron images of monazite grains; (b) chondrite-normalized monazite rare-earth elements; (c) Wetherill diagram with monazite U–Pb data; (d) backscatter electron image of xenotime grain; (e) chondrite-normalized xenotime rare-earth elements; (f) Wetherill diagram with xenotime U–Pb data. Ellipses-errors and uncertainties are stated at 2σ level. Chondrite normalization values from McDonough and Sun [89]. Average ages were constructed using the $^{206}\text{Pb}/^{238}\text{U}$ ages.

also have a NNW trend, orthogonal to the types 1 and 3 shear zones, as in the Itaiacoca Group [104] and in the Votuverava Group in the vicinity of Pilar do Sul city (SW São Paulo) [25, 33].

The quantified strain ellipsoids from all type 2 shear zones are prolate-shaped (Figure 11). On the other hand, transpressional zones with vertical foliation and down-dip stretching lineation are predicted to be pure shear-dominated with oblate-shaped ellipsoids (e.g., [61]), with many natural examples described in the literature; for example, the northern termination of the Itapirapuá shear zone [31], the Vermilion, Rosy Finch-Gem Lake and Western Idaho shear zones, United States of America [105–107], the Pelagonian Fault, Greece [108], the Alhama de Murcia Fault, Spain (Alonso-Henar et al., 2020), and the Zagros Transpressional Zone, Iran [109]. Samples from the internal domains of the Lajeado Group present coexisting plane strain and prolate-shaped ellipsoids of low to very low strain values, dominantly with high-angle stretching lineations. In this scenario, the prolate-shaped ellipsoids in type 2 shear zones can be explained by a superposition of two approximately plane strain fabrics associated with progressive deformation: a first associated with folding (pure shear-dominated) followed by thrusting (simple shear-dominated). Kinematic vorticity data for a representative sample from the Figueira shear zone (type 2) indicate

~41–58% pure shear component (Table 4; Figure 14, sample F196). Most type 2 shear zones present NW-dipping mylonitic foliation, top-to-the-SE kinematic indicators observed on vertical XZ sections of the strain ellipsoid, and sinistral sense of shear on horizontal YZ sections (e.g., Figueira and Agudos Grandes shear zones). However, the Ivaporunduva shear zone has a SE-dipping mylonitic foliation, top-to-the-NW kinematic indicators on XZ sections, and dextral indicators in YZ sections. Additionally, the domain limited by the Ivaporunduva and Piririca shear zones presents a higher metamorphic grade than the surrounding rocks (Figure 4), suggesting this domain underwent a vertical extrusion, a pattern expected for pure shear-dominated transpression.

Measured strain ellipsoids are exclusively oblate-shaped along the Ribeira shear zone (Figure 11), and kinematic vorticity data from rigid grain rotation and δ/β methods indicate a variable pure shear component ranging from ~9 to 72%, with a general dominance of a simple shear component (Table 4). Combined with a dominance of subhorizontal stretching lineation (Figure 3), and consistent dextral kinematic indicators observed at all scales (Figures 2, 4, and 7), these data suggest a subsimple shear deformation [3, 25].

Other strain models are also possible to explain the prolate/oblate strain ellipsoids. Prolate to oblate strain ellipsoids can be achieved by progressive deformation in low deformed

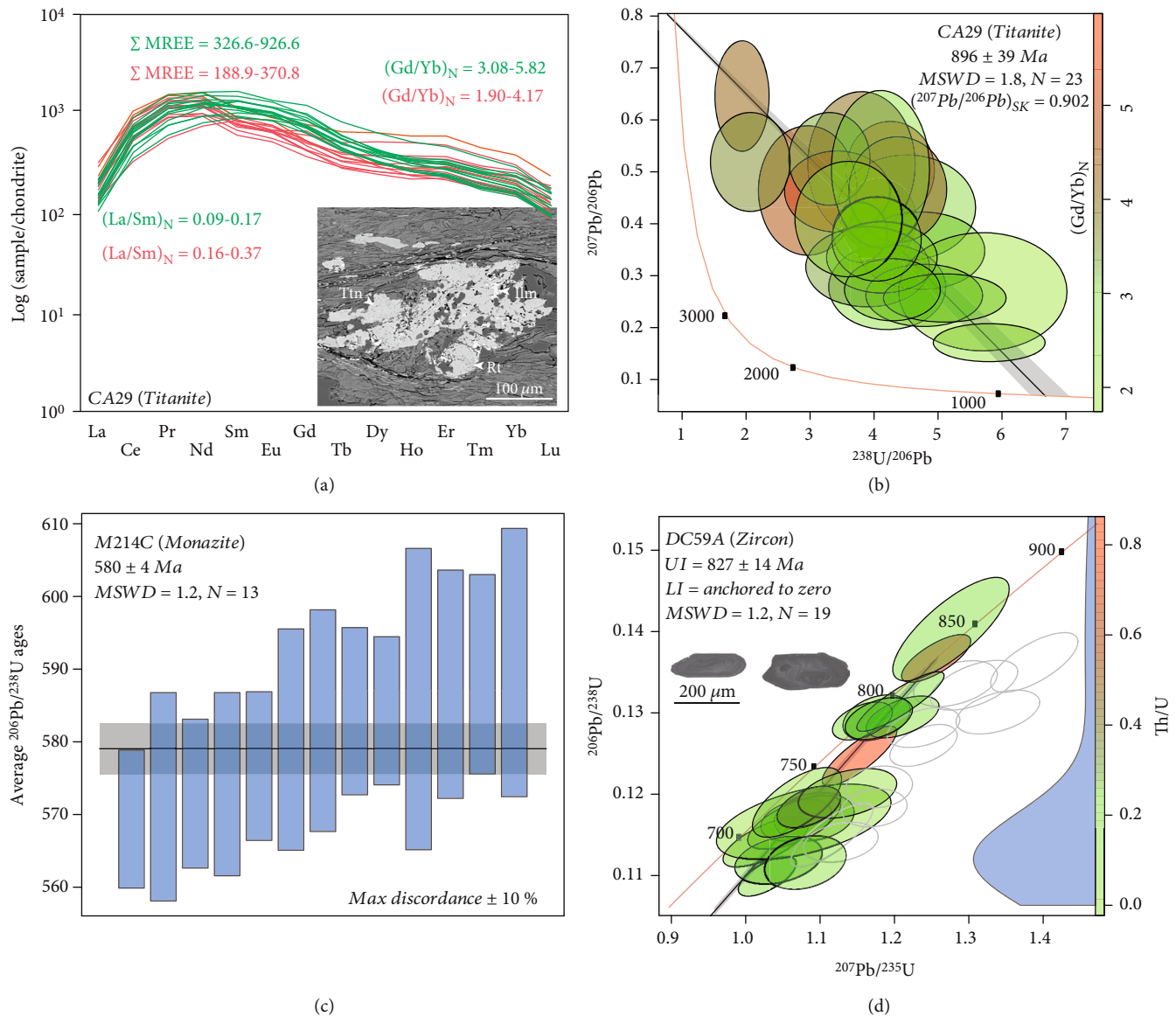


FIGURE 16: Geochronological data from rocks associated with the Itapirapuã (sample CA29) and Ribeira shear zones (samples M214C and DC59A). (a) Chondrite-normalized titanite rare-earth elements; (b) Tera-Wasserburg diagram with titanite U–Pb; (c) average ²⁰⁶Pb/²³⁸U monazite ages (maximum discordance of ±10%); (d) Wetherill diagram with zircon U–Pb data defining an upper intercept age (anchored to zero). Ellipses-errors and uncertainties are stated at 2 σ level. Chondrite normalization values from McDonough and Sun [89].

metasedimentary rocks, as the case of Lajeado Group domain, if a previous sedimentary oblate fabric is submitted to a vertical plane strain [60]. Oblate strain fabric with oblique stretching lineations is also predicted in numerical modelling of thrust, followed by wrench, shear zones [110], which could be the case for the type 2 zones followed by the NE and ENE (types 1 and 3) shear zones.

The Morro Agudo shear zone is the only type 4 structure present in the study area. At a first approximation, types 3 and 4 shear zones could be explained by a conjugate dextral/sinistral shear system. However, the angle between the two systems of the compressional dihedral is of 100–120°, which is not compatible with the classical shear failure criteria [60]. This could be explained by a conjugate set of shear structures developed under plasticity conditions, initially

formed with a dihedral angle of 90° that would tend to increase with the continuation of progressive ductile deformation [60].

5.3. Timing of Deformation along the Shear Zones. Previously published zircon, monazite, and apatite U–Pb, muscovite ⁴⁰Ar/³⁹Ar, and hornblende/biotite K–Ar geochronological data for shear zone-related rocks from the Ribeira Belt (Figure 17) suggest that main ductile episodes occurred between 610 and 500 Ma along the NE-trending orogen-parallel transcurrent shear zones [14, 30, 32, 35–37, 111–115]. Geochronological data from the Cubatão and Além Paraíba-Pádua shear zones indicate high-temperature ductile deformation at 610–570 Ma [35, 37]. The Taxaquara shear zone presents a well-constrained medium-temperature

evolution between 560 and 535 Ma, recorded in apatite U–Pb and syn-kinematic muscovite $^{40}\text{Ar}/^{39}\text{Ar}$ ages [33, 34]. Fine-fraction illite K–Ar data indicate brittle activities at 402 ± 6 Ma and 311 ± 8 Ma in the Camburu shear zone, an orogen-parallel transcurrent structure cutting the Costeiro-Oriental Terrane [38]. These data indicate that the shear zone system was active, probably intermittently, over at least ca. 300 Ma.

The new geochronological data obtained in this work indicate a longer and more complex deformational history beginning in early Tonian. Tonian U–Pb ages of 896 ± 39 Ma (titanite, CA29) and 829 ± 18 Ma (monazite, P33) were obtained from samples of the Itapirapuã shear zone (type 1 structure) (Figure 1(c)). Titanite in sample CA29 occurs as euhedral porphyroblasts with asymmetric strain shadows with dextral shear sense and wavy mineral inclusion trails in continuity with the external matrix foliation (Figure 16(a), inset), indicating a syn-kinematic metamorphic origin. Mineral equilibria and thermodynamic models indicate that sample CA29 attained peak metamorphic conditions of 490–510°C and 11–12.5 kbar represented by the assemblage chlorite–biotite–phengite–quartz–titanite–epidote–ilmenite [31]. These conditions indicate a transitional blueschist/low-temperature eclogite facies condition. The monazite U–Pb age of 829 ± 18 Ma is associated with cores of monazite from the mylonitic paragneiss sample P33, whereas monazite rims yielded a younger age of 675 ± 7 Ma (Figures 15(c)–15(f)). Considering that the Itapirapuã shear zone represents the boundary between Calymmian rocks of the Água Clara Formation (ca. 1590–1470 Ma; [56]) and the early Tonian rocks of the Itaiacoca Group (1030–910 Ma; [59]), the available geochronological and petrological data suggest a suture zone active between ca. 900 and 830 Ma. Younger episodes of ductile reactivation of the Itapirapuã shear zone are recorded in the monazite rims from sample P33 (675 ± 7 Ma) and in mylonitization of granitic rocks from the Três Córregos Suite (zircon U–Pb crystallization age of 600 ± 6 Ma; [116]). The zircon U–Pb age of 827 ± 14 Ma obtained for sample DC59A from the Ribeira shear zone belongs to a distinct geological context. This sample comes from an elongated body of mylonitic quartzite from the Serra das Andorinhas Formation (a unit of the Votuverava Group) at the interference zone between the Ribeira and Lancinha shear zones (Figure 2), thus representing an intraterrane geological context. The metamorphic origin of dated zircon is inferred from the dominance of Th/U below 0.1, its internal textures, and from the detrital zircon record of the same outcrop, characterized by U–Pb ages spanning 1910–2240 Ma and 2550–2730 Ma and the absence of ages younger than Paleoproterozoic [117].

A partially coeval Tonian (850–760 Ma) regional metamorphic event is recorded in rocks from the Embu Terrane, which also affected Calymmian rocks from the Votuverava Group (deposition at ca. 1450–1500 Ma; [43]) along the contact zone between the two units [39, 40]. This scenario suggests the onset of terrane assembly in the early Tonian, with nucleation of some orogen-parallel shear zones (e.g., Itapirapuã shear zone) and some intraterrane shear zones cutting Calymmian rocks from the Apiaí Terrane (e.g., Ribeira shear

zone). Younger ductile deformation along the Ribeira shear zone is recorded in the monazite U–Pb age of 580 ± 4 Ma for sample M214C (Figure 16(c)) and for mylonitization of rocks from the Itaoca Granite (zircon U–Pb crystallization age of 612 ± 3 Ma; [116]; see Figures 2 and 4).

Field relationships indicate that the intraterrane type 2 shear zones within the Lajeado Group were active before 612 ± 3 Ma, as they were cut by the Itaoca Granite (Figures 2 and 4). On the other hand, the Figueira and Agudos Grandes shear zones deformed metaconglomerates containing granitic pebbles with a zircon U–Pb age of 593 ± 15 Ma and volcanic rocks with zircon U–Pb age of 579 ± 34 Ma from the Iporanga Formation [42]. Although the maximum deformation time is unconstrained, these data suggest a long-lived history for the intraterrane reverse shear zones within the Apiaí Terrane.

Data on anisotropy of magnetic susceptibility and zircon U–Pb ages from granitic plutons emplaced in the Apiaí Terrane suggest a coherent syntectonic context with individual plutons developed during stages of folding and transpression (615–600 Ma) and transtension (597–588 Ma, A-type extensional granites) [116, 125]. These data were used to interpret the onset of the ductile transpressional deformation at ca. 595 Ma [125], but our data indicate a more complex deformation history.

In summary, the combination of our new and published geochronological data suggests intermittent ductile shear zone activity from ca. 900–830 Ma to 500 Ma. During this period, shearing deformation was coeval to at least two major episodes of terrane accretion at 850–760 Ma (metamorphism recorded in the Embu Complex and Votuverava Group, northward of the Lancinha-Cubatão shear zone; [39, 40]) and 610–585 Ma (high-pressure metamorphism recorded in the Turvo-Cajati Formation, southward of the Lancinha-Cubatão shear zone; [14, 15, 41]). Geochronological and petrological data suggest that suture zones of Tonian ages occur along the contacts between the Apiaí and Embu terranes (Votuverava Group and Embu Complex, Figure 1(c)) and along the Itapirapuã shear zone ([31, 39], this work). A main Ediacaran suture zone is represented by the Lancinha-Cubatão shear zone that separates the Curitiba and Costeiro terranes to the south and the Apiaí and Embu terranes to the north ([37, 41]). In this scenario, the ductile deformation between 560 and 535 Ma was recorded in the Taxaquara shear zone [33, 34], and younger brittle reactivations [38] and postdate terrane assembly are best inferred as late-stage, intracontinental reactivations of the shear zone system.

6. Conclusions

This work presents a comprehensive multiscale analysis of the complex shear zone system from the Ribeira Belt, SE Brazil, unravelling the thermal and deformation regimes and the timing of deformation based on the character of, and interplay between, multiple shear zones. The combination of microstructural data with mineral assemblages and thermobarometric conditions indicates a transitional north-eastward increase in metamorphic conditions from lower

greenschist to granulite facies conditions (up to $\sim 750^{\circ}\text{C}$), reflecting the different crustal levels in which each shear zone developed. Strain data suggest that the shear zone system was not developed in a single transpressional stage, but by a major episode of thrusting followed by the development of strike-slip shear zones dominated by a subsimple shear strain regime.

This study reveals that the shear zone system of the Ribeira Belt underwent a long-lived development, which is in contrary to previous suggestions (e.g., [26]). The new geochronological data presented here and those available in the literature suggest intermittent ductile shear zone activations from ca. 900–830 Ma to 500 Ma, coeval with at least two major episodes of terrane accretion at 850–760 Ma and 610–585 Ma, the last associated with the main stage of Gondwana assembly. The anastomosing shear zone system was probably active at 610–585 Ma. Additionally, the combination of geochronological data with thermobarometric estimates indicates that some of the shear zones represent suture zones (e.g., Itapirapuã shear zone), whereas others represent intraterrane shear zones (e.g., Ribeira, Figueira, and Agudos Grandes shear zones) and postcollisional shear zones (e.g., Taxaquara shear zone) reactivated in an intracontinental setting (560–535 Ma).

Data Availability

Supporting data is available at Figshare repository: <https://figshare.com/s/026ec5cbfb2c57308f7e>.

Conflicts of Interest

The authors declare that they have no known competing financial interests or personal relationships that could have appeared to influence the work reported in this paper.

Acknowledgments

Financial support was provided by grants 01/00199-4, 2018/10012-0, 2019/10457-4, and 2015/26645-3, São Paulo Research Foundation (FAPESP). FMF and GACC thank the research productivity scholarship grants 307732/2019-3 and 305701/2019-3, National Council of Technological and Scientific Development (CNPq). BVR and PAC acknowledge financial support from the Australian Research Council (ARC) grant FL160100168.

Supplementary Materials

U–Pb–REE data and standard analyses. (*Supplementary Materials*)

References

- [1] J. G. Ramsay, “Shear zone geometry: a review,” *Journal of Structural Geology*, vol. 2, pp. 83–99, 1980.
- [2] G. I. Alsop and R. E. Holdsworth, “The geometry and topology of natural sheath folds: a new tool for structural analysis,” *Journal of Structural Geology*, vol. 26, pp. 1561–1589, 2004.
- [3] H. Fossen and G. C. G. Cavalcante, “Shear zones – a review,” *Earth-Science Reviews*, vol. 171, pp. 434–455, 2017.
- [4] R. J. Norris and V. G. Toy, “Continental transforms: a view from the alpine fault,” *Journal of Structural Geology*, vol. 64, pp. 3–31, 2014.
- [5] K. Scharer and A. Streig, “The San Andreas fault system: complexities along a major transform fault system and relation to earthquake hazards,” in *Transform Plate Boundaries and Fracture Zones*, J. C. Duarte, Ed., pp. 249–269, Elsevier, 2019.
- [6] D. G. Howell, “Principles of terrane analysis: new applications for global tectonics,” in *Topics in the Earth Sciences Vol. 8*, p. 262, Chapman and Hall, London, Second edition, 1995.
- [7] N. Woodcock and C. Schubert, “Continental strike-slip tectonics,” in *Continental Deformation*, P. L. Hancock, Ed., pp. 251–263, Pergamon Press, New York, 1994.
- [8] V. G. Toy, D. J. Prior, and R. J. Norris, “Quartz fabrics in the alpine fault mylonites: influence of pre-existing preferred orientations on fabric development during progressive uplift,” *Journal of Structural Geology*, vol. 30, pp. 602–621, 2008.
- [9] B. B. Brito Neves, M. C. Campos Neto, and R. A. Fuck, “From Rodinia to western Gondwana: an approach to the Brasiliano-Pan African cycle and orogenic collage,” *Episodes*, vol. 22, no. 3, pp. 155–166, 1999.
- [10] M. Heilbron and N. Machado, “Timing of terrane accretion in the Neoproterozoic-Eopaleozoic Ribeira orogen (se Brazil),” *Precambrian Research*, vol. 125, pp. 87–112, 2003.
- [11] G. A. C. Campanha and B. B. Brito Neves, “Frontal and oblique tectonics in the Brazilian shield,” *Episodes*, vol. 27, no. 4, pp. 255–259, 2004.
- [12] M. Heilbron, A. C. Pedrosa-Soares, M. C. Campos Neto, L. C. Silva, R. A. Trouw, and V. A. Janasi, “Província Mantiqueira,” in *Geology of South American Continent: Evolution of the Work of Fernando Flávio Marques de Almeida*, pp. 203–234, 2004.
- [13] M. Heilbron, A. Ribeiro, C. M. Valeriano et al., “The Ribeira belt,” in *Tectonic Genealogy of a Miniature Continent*, M. Heilbron, U. Cordani, and F. F. Alkmim, Eds., vol. 1pp. 277–304, Springer, Cham, 1st edition, 2017.
- [14] F. M. Faleiros, G. A. C. Campanha, L. Martins, S. R. F. Vlach, and P. M. Vasconcelos, “Ediacaran high-pressure collision metamorphism and tectonics of the southern Ribeira Belt (SE Brazil): evidence for terrane accretion and dispersion during Gondwana assembly,” *Precambrian Research*, vol. 189, no. 3-4, pp. 263–291, 2011.
- [15] F. M. Faleiros, G. A. C. Campanha, M. Pavan, V. V. Almeida, S. W. O. Rodrigues, and B. P. Araújo, “Short-lived polyphase deformation during crustal thickening and exhumation of a collisional orogen (Ribeira belt, Brazil),” *Journal of Structural Geology*, vol. 93, pp. 106–130, 2016.
- [16] V. T. Meira, A. Garcia-Casco, C. Juliani, R. P. Almeida, and J. H. D. Schorscher, “The role of intracontinental deformation in supercontinent assembly: insights from the Ribeira belt, southeastern Brazil (Neoproterozoic West Gondwana),” *Terra Nova*, vol. 27, pp. 206–217, 2015.
- [17] V. T. Meira, A. Garcia-Casco, T. Hyppolito, C. Juliani, and J. H. D. Schorscher, “Tectono-metamorphic evolution of the central Ribeira belt, Brazil: a case of late Neoproterozoic intracontinental orogeny and flow of partially molten deep

- crust during the assembly of West Gondwana,” *Tectonics*, vol. 38, pp. 3182–3209, 2019.
- [18] V. T. Meira, A. Garcia-Casco, C. Juliani, and J. H. D. Schorscher, “Late Tonian within-plate mafic magmatism and Ediacaran partial melting and magmatism in the Costeiro Domain, Central Ribeira Belt, Brazil,” *Precambrian Research*, vol. 334, article 105440, 2019.
- [19] J. Konopásek, G. C. G. Cavalcante, H. Fossen, and V. Janousek, “Adamastor - an ocean that never existed?,” *Earth-Science Reviews*, vol. 205, article 103201, 2020.
- [20] G. R. Sadowski, “A megafalha de Cubatão no sudeste brasileiro,” *Boletim IG-USP, Série Científica*, vol. 22, pp. 15–28, 1991.
- [21] M. Egydio-Silva, A. Vauchez, J. Bascou, and J. Hippertt, “High-temperature deformation in the Neoproterozoic transpressional Ribeira belt, Southeast Brazil,” *Tectonophysics*, vol. 352, pp. 203–224, 2002.
- [22] F. M. Faleiros, G. A. C. Campanha, R. M. S. Bello, and K. Fuzikawa, “Quartz recrystallization regimes, c -axis texture transitions and fluid inclusion reequilibration in a prograde greenschist to amphibolite facies mylonite zone (Ribeira Shear Zone, SE Brazil),” *Tectonophysics*, vol. 485, no. 1–4, pp. 193–214, 2010.
- [23] D. Cabrita, E. Salamuni, and L. Lagoeiro, “Fabric evolution of polydeformed orthogneisses and quartzites along the Curitiba shear zone, Curitiba domain, southern Brazil,” *Journal of South American Earth Sciences*, vol. 77, pp. 206–217, 2017.
- [24] C. Cavalcante, L. Lagoeiro, H. Fossen et al., “Temperature constraints on microfabric patterns in quartzofeldspathic mylonites, Ribeira belt (SE Brazil),” *Journal of Structural Geology*, vol. 115, pp. 243–262, 2018.
- [25] B. V. Ribeiro, F. M. Faleiros, G. A. C. Campanha, L. Lagoeiro, R. F. Weinberg, and N. J. R. Hunter, “Kinematics, nature of deformation and tectonic setting of the Taxaquara shear zone, a major transpressional zone of the Ribeira belt (SE Brazil),” *Tectonophysics*, vol. 751, pp. 83–108, 2019.
- [26] T. Conte, C. Cavalcante, L. E. Lagoeiro, H. Fossen, and C. S. Silveira, “Quartz textural analysis from an anastomosing shear zone system: implications for the tectonic evolution of the Ribeira belt, Brazil,” *Journal of South American Earth Sciences*, vol. 103, article 102750, 2020.
- [27] F. M. Faleiros, G. A. C. Campanha, R. M. S. Bello, and K. Fuzikawa, “Fault-valve action and vein development during strike-slip faulting: An example from the Ribeira Shear Zone, Southeastern Brazil,” *Tectonophysics*, vol. 438, no. 1–4, pp. 1–32, 2007.
- [28] A. M. Faleiros, G. A. C. Campanha, F. M. Faleiros, and R. M. S. Bello, “Fluid regimes, fault-valve behavior and formation of gold-quartz veins – The Morro do Ouro Mine, Ribeira Belt, Brazil,” *Ore Geology Reviews*, vol. 56, pp. 442–456, 2014.
- [29] I. S. Malta, F. M. Faleiros, L. V. S. Monteiro, M. B. Andrade, B. Codebella, and M. C. B. Esteves, “P-T-fluid-deformation regime of the Ediacaran Serra do Cavalo Magro orogenic gold deposit, Ribeira belt, Brazil,” *Ore Geology Reviews*, vol. 120, article 103384, 2020.
- [30] C. R. Passarelli, M. A. S. Basei, K. Wemmer, O. Siga Jr., and P. Oyhantçabal, “Major shear zones of southern Brazil and Uruguay: escape tectonics in the eastern border of Rio de La plata and Paranapanema cratons during the Western Gondwana amalgamation,” *International Journal of Earth Sciences*, vol. 100, pp. 391–414, 2011.
- [31] A. J. Forero-Ortega, G. A. C. Campanha, F. M. Faleiros, and M. T. A. G. Yogi, “Pure shear-dominated transpression and vertical extrusion in a strike-slip fault splay from the Itapirapua Shear Zone, Ribeira Belt, Brazil,” *Tectonophysics*, vol. 786, article 228455, 2020.
- [32] R. Machado, N. M. Dehler, and P. Vasconcelos, “ $^{40}\text{Ar}/^{39}\text{Ar}$ ages (600–570 Ma) of the Serra do Azeite transtensional shear zone: evidence for syncontractional extension in the Cajati area, southern Ribeira belt,” *Anais da Academia Brasileira Ciências*, vol. 79, no. 4, pp. 713–723, 2007.
- [33] B. V. Ribeiro, J. A. Mulder, F. M. Faleiros et al., “Using apatite to resolve the age and protoliths of mid-crustal shear zones: a case study from the Taxaquara shear zone, SE Brazil,” *Lithos*, vol. 378–379, article 105817, 2020.
- [34] B. V. Ribeiro, L. Lagoeiro, F. M. Faleiros et al., “Strain localization and fluid-assisted deformation in apatite and its influence on trace elements and U-Pb systematics,” *Earth and Planetary Science Letters*, vol. 545, article 116421, 2020.
- [35] S. J. Giraldo, R. A. J. Trouw, P. Duffles, R. V. Costa, M. I. Mejia, and R. S. Marimon, “Structural analysis combined with new geothermobarometric and geochronological results of the Alem Paraiba shear zone, between Tres Rios and Bananal, Ribeira Orogen, SE Brazil,” *Journal of South American Earth Sciences*, vol. 90, pp. 118–136, 2019.
- [36] R. V. Costa, R. A. J. Trouw, R. S. Marimon, F. Nepomuceno, J. C. Mendes, and E. Dantas, “Sao Bento do Sapucaí Shear Zone: Constraining age and P-T conditions of a collisional Neoproterozoic oblique shear zone, Ribeira Orogen, Brazil,” *Journal of South American Earth Sciences*, vol. 98, article 102418, 2020.
- [37] D. I. G. Cabrita, F. M. Faleiros, L. Menegon, B. V. Ribeiro, P. A. Cawood, and G. A. C. Campanha, “Deformation, thermochronology and tectonic significance of the crustal-scale Cubatão Shear Zone, Ribeira belt, Brazil,” *Tectonophysics*, 2021.
- [38] C. A. S. Mora, G. A. C. Campanha, and K. Wemmer, “Microstructures and K-Ar illite fine-fraction ages of the cataclastic rocks associated to the Camburu shear zone, Ribeira belt, southeastern Brazil,” *Brazilian Journal of Geology*, vol. 43, no. 4, pp. 607–622, 2013.
- [39] G. A. C. Campanha, F. M. Faleiros, P. A. Cawood, D. I. G. Cabrita, B. V. Ribeiro, and M. A. S. Basei, “The Tonian Embu complex in the Ribeira belt (Brazil): revision, depositional age and setting in Rodinia and West Gondwana,” *Precambrian Research*, vol. 320, pp. 31–45, 2019.
- [40] D. I. G. Cabrita, F. M. Faleiros, P. A. Cawood et al., “Petrochronological constraints and tectonic implications of Tonian metamorphism in the Embu complex, Ribeira belt, Brazil,” *Precambrian Research*, vol. 363, article 106315, 2021.
- [41] B. S. Ricardo, F. M. Faleiros, R. Moraes, R. O. Siga Júnior, and G. A. C. Campanha, “Tectonic implications of juxtaposed high- and low-pressure metamorphic field gradient rocks in the Turvo-Cajati formation, Curitiba terrane, Ribeira belt, Brazil,” *Precambrian Research*, vol. 345, p. 105766, 2020.
- [42] G. A. C. Campanha, M. S. Basei, C. C. G. Tassinari, A. P. Nutman, and F. M. Faleiros, “Constraining the age of the Iporanga Formation with SHRIMP U-Pb zircon: Implications for possible Ediacaran glaciation in the Ribeira Belt, SE Brazil,” *Gondwana Research*, vol. 13, no. 1, pp. 117–125, 2008.
- [43] G. A. C. Campanha, F. M. Faleiros, M. A. S. Basei, C. C. G. Tassinari, A. P. Nutman, and P. M. Vasconcelos,

- “Geochemistry and age of mafic rocks from the Votuverava Group, southern Ribeira Belt, Brazil: Evidence for 1490 Ma oceanic back-arc magmatism,” *Precambrian Research*, vol. 266, pp. 530–550, 2015.
- [44] G. A. C. Campanha, M. A. S. Basei, F. M. Faleiros, and A. P. Nutman, “The Mesoproterozoic to early Neoproterozoic passive margin Lajeado Group and Apiai Gabbro, Southeastern Brazil,” *Geoscience Frontiers*, vol. 7, no. 4, pp. 683–694, 2016.
- [45] C. Valeriano, “The southern Brasília belt,” in *Regional Geology Reviews* Springer, Cham.
- [46] R. Henrique-Pinto, M. A. S. Basei, P. R. Santos et al., “Paleozoic Paraná Basin transition from collisional retro-foreland to pericratonic syncline: implications on the geodynamic model of Gondwana proto-Andean margin,” *Journal of South American Earth Sciences*, vol. 111, article 103511, 2021.
- [47] L. A. Hartmann, J. O. S. Santos, N. J. McNaughton, M. A. Z. Vasconcelos, and L. C. Silva, “Ion microprobe (SHRIMP) dates complex granulite from Santa Catarina, southern Brazil,” *Anais da Academia Brasileira de Ciências*, vol. 72, no. 4, pp. 559–572, 2000.
- [48] M. A. S. Basei, A. Nutman, O. Siga Júnior, C. R. Passarelli, and C. O. Drukas, “Chapter 7.2 The Evolution and Tectonic Setting of the Luis Alves Microplate of Southeastern Brazil: An Exotic Terrane during the Assembly of Western Gondwana,” *Developments in Precambrian Geology*, vol. 16, pp. 273–291, 2009.
- [49] O. Siga Júnior, *Tectonic domains of southeastern Paraná and northeastern Santa Catarina: geochronology and crustal evolution*, PhD Thesis, University of São Paulo, 1995.
- [50] V. A. Janasi, R. J. Leite, and W. R. Van Schmus, “U-Pb chronostratigraphy of the granitic magmatism in the Agudos Grandes Batholith (west of Sao Paulo, Brazil) – implications for the evolution of the Ribeira Belt,” *Journal of South American Earth Sciences*, vol. 14, no. 4, pp. 363–376, 2001.
- [51] L. C. Silva, N. J. McNaughton, R. Armstrong, L. A. Hartmann, and I. R. Fletcher, “The neoproterozoic Mantiqueira Province and its African connections: a zircon-based U-Pb geochronologic subdivision for the Brasiliano/Pan-African systems of orogens,” *Precambrian Research*, vol. 136, no. 3-4, pp. 203–240, 2005.
- [52] R. J. Leite, L. M. Heaman, V. A. Janasi, L. Martins, and R. A. Creaser, “The late- to postorogenic transition in the Neoproterozoic Agudos Grandes Granite Batholith (Apiai Domain, SE Brazil): Constraints from geology, mineralogy, and U-Pb geochronology,” *Journal of South American Earth Sciences*, vol. 23, no. 2-3, pp. 193–212, 2007.
- [53] A. Alves, V. A. Janasi, M. C. Campos Neto, L. Heaman, and A. Simonetti, “U-Pb geochronology of the granite magmatism in the Embu terrane: implications for the evolution of the central Ribeira belt, SE Brazil,” *Precambrian Research*, vol. 230, pp. 1–12, 2013.
- [54] M. Heilbron, C. M. Valeriano, C. Peixoto et al., “Neoproterozoic magmatic arc systems of the central Ribeira belt, SE-Brazil, in the context of the West-Gondwana pre-collisional history: a review,” *Journal of South American Earth Sciences*, vol. 105, article 102710, 2020.
- [55] L. F. Cury, G. A. Kaulfuss, O. Siga Junior, M. A. S. Basei, O. M. M. Harara, and K. Sato, “Idades U-Pb (Zircões) de 1.75 Ga em granitóides alcalinos deformados dos núcleos Betara e Tigre: evidências de regimes extensionais do estateriano na Faixa Apiai,” *Geologia USP-Série Científica*, vol. 2, no. 1, pp. 95–108, 2002.
- [56] W. Weber, O. Siga Junior, K. Sato, J. M. Reis Neto, M. A. S. Basei, and A. P. Nutman, “A Formação Água Clara na Região de Araçáiba - SP: registro U-Pb de uma bacia mesoproterozóica,” *Geologia USP-Série Científica*, vol. 4, no. 1, pp. 101–110, 2004.
- [57] V. Maniesi, *Petrology of amphibolite rocks from the regions of Adrianópolis, Campo Largo and Rio Branco do Sul/PR*, PhD Thesis, Institute of Geosciences and Exact Sciences, São Paulo State University, Rio Claro, 1997.
- [58] M. T. A. G. Yogi, *Thermobaric and kinematic evolution of Anta Gorda Anticlinorium, Ribeira belt: metamorphism record and shear deformation in a transpressional setting*, Master Thesis, São Paulo University, 2019.
- [59] O. Siga Jr., M. A. S. Basei, C. R. Passarelli, K. Sato, L. F. Cury, and I. McCreath, “Lower and Upper Neoproterozoic magmatic records in Itaiacoca Belt (Parana- Brazil): Zircon ages and lithostratigraphy studies,” *Gondwana Research*, vol. 15, no. 2, pp. 197–208, 2009.
- [60] J. G. Ramsay and M. I. Huber, “The Techniques of Modern Structural Geology, Volume 1: Strain Analysis,” Academic press, 1983.
- [61] D. J. Sanderson and W. R. D. Marchini, “Transpression,” *Journal of Structural Geology*, vol. 6, pp. 449–458, 1984.
- [62] J. E. Dewey, R. E. Holdsworth, and R. A. Strachan, “Transpression and transtension zones,” in *Continental Transpressional and Transtensional Tectonics*, Geological Society, R. E. Holdsworth, R. A. Strachan, and J. E. Dewey, Eds., vol. 135, pp. 1–14, Special Publications, London, 1998.
- [63] P. Y. F. Robin and A. R. Cruden, “Strain and vorticity patterns in ideally ductile transpression zones,” *Journal of Structural Geology*, vol. 16, pp. 447–466, 1994.
- [64] R. R. Jones, R. E. Holdsworth, and W. Bailey, “Lateral extrusion in transpression zones: the importance of boundary conditions,” *Journal of Structural Geology*, vol. 19, pp. 1201–1217, 1997.
- [65] P. Launeau and A. R. Cruden, “Magmatic fabric acquisition mechanisms in a syenite: results of a combined anisotropy of magnetic susceptibility and image analysis study,” *Journal of Geophysical Research*, vol. 103, pp. 5067–5089, 1998.
- [66] P. Launeau and P. Y. F. Robin, *SPO software*, Université de Nantes (France)/ University of Toronto (Canada), 2003, <http://www.sciences.univ-nantes.fr/geol/UMR6112/SPO/SPO.html>.
- [67] P. P. Launeau and P. Y. F. Robin, “Determination of fabric and strain ellipsoids from measured sectional ellipses – implementation and applications,” *Journal of Structural Geology*, vol. 27, no. 12, pp. 2223–2233, 2005.
- [68] P. Y. F. Robin, “Determination of fabric and strain ellipsoids from measured sectional ellipses—theory,” *Journal of Structural Geology*, vol. 24, pp. 531–544, 2002.
- [69] J. G. Ramsay and M. I. Huber, *The Techniques of Modern Structural Geology, Volume 2: Folds and Fractures*, Academic Press, 1987.
- [70] C. W. Passchier, “Analysis of deformation paths in shear zones,” *Geologische Rundschau*, vol. 77, pp. 309–318, 1988.
- [71] C. W. Passchier, “Stable positions of rigid objects in non-coaxial flow—a study in vorticity analysis,” *Journal of Structural Geology*, vol. 9, pp. 679–690, 1987.
- [72] S. Wallis, “Vorticity analysis and recognition of ductile extension in the Sanbagawa belt, SW Japan,” *Journal of Structural Geology*, vol. 17, pp. 1077–1093, 1995.

- [73] N. J. R. Hunter, R. F. Weinberg, C. J. L. Wilson, and R. D. Law, "A new technique for quantifying symmetry and opening angles in quartz c-axis pole figures: implications for interpreting the kinematic and thermal properties of rocks," *Journal of Structural Geology*, vol. 112, pp. 1–6, 2018.
- [74] M. Wiedenbeck, P. Allé, F. Corfu et al., "Three natural zircon standards for U-Th-Pb, Lu-Hf, trace element and REE analyses," *Geostandards Newsletter*, vol. 19, no. 1, pp. 1–23, 1995.
- [75] J. L. Payne, M. Hand, K. M. Barovich, and B. P. Wade, "Temporal constraints on the timing of high-grade metamorphism in the northern Gawler craton: implications for assembly of the Australian Proterozoic," *Australian Journal of Earth Sciences*, vol. 55, pp. 623–640, 2008.
- [76] J. N. Aleinikoff, R. P. Wintsch, R. P. Tollo, D. M. Unruh, C. M. Fanning, and M. D. Schmitz, "Ages and origins of rocks of the Killingworth dome, south-central Connecticut: implications for the tectonic evolution of southern New England," *American Journal of Science*, vol. 307, pp. 63–118, 2007.
- [77] S. E. Jackson, N. J. Pearson, W. L. Griffin, and E. A. Belousova, "The application of laser ablation-inductively coupled plasma-mass spectrometry to in situ U–Pb zircon geochronology," *Chemical Geology*, vol. 211, pp. 47–69, 2004.
- [78] J. Slama, J. Kosler, D. J. Condon et al., "Plešovice zircon – A new natural reference material for U-Pb and Hf isotopic microanalysis," *Chemical Geology*, vol. 249, no. 1–2, pp. 1–35, 2008.
- [79] R. A. Stern, S. Bodorkos, S. L. Kamo, A. H. Hickman, and F. Corfu, "Measurement of SIMS instrumental mass fractionation of Pb isotopes during zircon dating," *Geostandards and Geoanalytical Research*, vol. 33, pp. 145–168, 2009.
- [80] L. P. Black, S. L. Kamo, I. S. Williams et al., "The application of SHRIMP to Phanerozoic geochronology: a critical appraisal of four zircon standards," *Chemical Geology*, vol. 200, pp. 171–188, 2003.
- [81] J. N. Aleinikoff, W. S. Schenck, M. O. Plank et al., "Deciphering igneous and metamorphic events in high-grade rocks of the Wilmington complex, Delaware: morphology, cathodoluminescence and backscattered electron zoning, and SHRIMP U-Pb geochronology of zircon and monazite," *Geological Society of America Bulletin*, vol. 118, pp. 39–64, 2006.
- [82] A. K. Kennedy, S. L. Kamo, L. Nasdala, and N. E. Timms, "Grenville skarn titanite: potential reference material for Sims U-Th-Pb analysis," *Canadian Mineralogist*, vol. 48, pp. 1423–1443, 2010.
- [83] C. Paton, J. D. Woodhead, J. C. Hellstrom, J. M. Hergt, A. Greig, and R. Maas, "Improved laser ablation U-Pb zircon geochronology through robust downhole fractionation correction," *Geochemistry, Geophysics, Geosystems*, vol. 11, article Q0AA06, 2010.
- [84] C. Paton, J. Hellstrom, B. Paul, J. Woodhead, and J. Hergt, "Iolite: freeware for the visualisation and processing of mass spectrometric data," *Journal of Analytical Atomic Spectrometry*, vol. 26, p. 2508, 2011.
- [85] P. Vermeesch, "IsoplotR: a free and open toolbox for geochronology," *Geoscience Frontiers*, vol. 9, pp. 1479–1493, 2018.
- [86] C. L. Kirkland, D. Fougereuse, S. M. Reddy, J. Hollis, and D. W. Saxey, "Assessing the mechanisms of common Pb incorporation into titanite," *Chemical Geology*, vol. 483, pp. 558–566, 2018.
- [87] S. N. Thomson, G. E. Gehrels, J. Ruiz, and R. Buchwaldt, "Routine low-damage apatite U-Pb dating using laser ablation-multicollector-ICPMS," *Geochemistry, Geophysics, Geosystems*, vol. 13, article Q0AA21, 2012.
- [88] J. S. Stacey and J. D. Kramers, "Approximation of terrestrial lead isotope evolution by a two-stage model," *Earth and Planetary Science Letters*, vol. 26, pp. 207–221, 1975.
- [89] W. F. McDonough and S. S. Sun, "The composition of the earth," *Chemical Geology*, vol. 120, no. 3–4, pp. 223–253, 1995.
- [90] I. S. Buick, C. Lana, and C. Gregory, "A LA-ICP-MS and SHRIMP U/Pb age constraint on the timing of REE mineralisation associated with Bushveld granites," *South African Journal of Geology*, vol. 114, pp. 1–14, 2011.
- [91] A. P. Fiori, "Preliminary assessment of the ductile displacement of the Lancinha and Morro Agudo faults in the state of Paraná," *Boletim Paranaense de Geociências*, vol. 36, pp. 15–20, 1985.
- [92] E. Fassbinder, "Structural analysis of the Lancinha Fault, Paraná State," MSc Dissertation, University of São Paulo, 1990.
- [93] G. A. C. Campanha and G. R. Sadowski, "Determinações Da Deformação Finita Em Rochas Metassedimentares Da Faixa Ribeira Na Região De Iporanga E Apiaí, Sp," *Revista Brasileira de Geociências*, vol. 32, no. 1, pp. 107–118, 2002.
- [94] C. A. Salazar, C. J. Archanjo, M. Babinski, and D. Liu, "Magnetic fabric and zircon U–Pb geochronology of the Itaoca pluton: implications for the Brasiliano deformation of the southern Ribeira belt (SE Brazil)," *Journal of South American Earth Sciences*, vol. 26, pp. 286–299, 2008.
- [95] V. Jelinek, "Characterization of the magnetic fabric of rocks," *Tectonophysics*, vol. 79, no. 3–4, pp. T63–T67, 1981.
- [96] M. Stipp, H. Stünitz, R. Heilbronner, and S. M. Schmid, "The eastern Tonale fault zone: a "natural laboratory" for crystal plastic deformation of quartz over a temperature range from 250 to 700 °C," *Journal of Structural Geology*, vol. 24, pp. 1861–1884, 2002.
- [97] H. Stipp, R. Stünitz, S. Heilbronner, and M. Schmid, "Dynamic recrystallization of quartz: correlation between natural and experimental conditions," in *Deformation Mechanisms, Rheology and Tectonics: Current Status and Future Perspectives*, Geological Society, S. Meer, M. R. Drury, J. H. P. Bresser, and G. M. Pennock, Eds., vol. 200, pp. 171–190, Special Publications, London, 2002.
- [98] D. Patias, L. F. Cury, F. M. Faleiros, M. Calderón, O. Siga Jr., and T. Theye, "Late Neoproterozoic P-T-t paths of syn- and post-collisional metamorphism in the Paranaçuá terrane, Ribeira belt (Brazil): implications for West Gondwana assembly," *International Geology Review*, vol. 63, no. 18, pp. 2314–2337, 2021.
- [99] H. D. Ebert and Y. Hasui, "Transpressional tectonics and strain partitioning during oblique collision between three plates in the Precambrian of southeast Brazil," in *Continental Transpressional and Transtensional Tectonics*, Geological Society, R. E. Holdsworth, R. A. Strachan, and J. F. Dewey, Eds., vol. 135, pp. 231–252, Special Publication, London, 1998.
- [100] W. B. Harland, "Tectonic transpression in Caledonian Spitsbergen," *Geological Magazine*, vol. 108, no. 1, pp. 27–41, 1971.
- [101] H. Fossen and B. Tikoff, "The deformation matrix for simultaneous simple shearing, pure shearing and volume change, and its application to transpression–transtension tectonics," *Journal of Structural Geology*, vol. 15, pp. 413–422, 1993.

- [102] B. Tikoff and H. Fossen, "Simultaneous pure and simple shear: the unifying deformation matrix," *Tectonophysics*, vol. 217, pp. 267–283, 1993.
- [103] B. Tikoff and C. Teyssier, "Strain modeling of displacement-field partitioning in transpressional orogens," *Journal of Structural Geology*, vol. 16, no. 11, pp. 1575–1588, 1994.
- [104] S. W. O. Rodrigues and F. P. Caltabeloti, *Geology and mineral resources of the Itararé Sheet - SG.22-X-B-I, 1:100,000 scale, São Paulo and Paraná states*, Geological Survey of Brazil – CPRM, Geology of Brazil Program – Basic Surveys, São Paulo, 2012.
- [105] P. J. Hudleston, D. Schultz-Ela, and D. L. Southwick, "Transpression in an Archean greenstone belt, northern Minnesota," *Canadian Journal of Earth Sciences*, vol. 25, pp. 1060–1068, 1988.
- [106] B. Tikoff and D. Greene, "Stretching lineations in transpressional shear zones: an example from the Sierra Nevada Batholith, California," *Journal of Structural Geology*, vol. 19, no. 1, pp. 29–39, 1997.
- [107] S. Giorgis, Z. Michels, L. Dair, N. Braudy, and B. Tikoff, "Kinematic and vorticity analyses of the western Idaho shear zone, USA," *Lithosphere*, vol. 9, no. 2, pp. 223–234, 2017.
- [108] P. Xypolias, S. Kokkalas, and K. Skourlis, "Upward extrusion and subsequent transpression as a possible mechanism for the exhumation of HP/LT rocks in Evia Island (Aegean Sea, Greece)," *Journal of Geodynamics*, vol. 35, pp. 303–332, 2003.
- [109] K. Sarkarinejad, "Quantitative finite strain and kinematic flow analyses along the Zagros transpression zone, Iran," *Tectonophysics*, vol. 442, pp. 49–65, 2007.
- [110] O. Merle and D. Gapais, "Strains within thrust-wrench zones," *Journal of Structural Geology*, vol. 19, pp. 1011–1014, 1997.
- [111] G. A. C. Campanha, "O Lineamento De Além-Paraíba NA ÁREA DE Três Rios (RJ)," *Revista Brasileira de Geociências*, vol. 11, no. 3, pp. 159–171, 1981.
- [112] P. C. Hackspacher, A. H. Fetter, W. Teixeira et al., "Final stages of the Brasiliano orogenesis in SE Brazil: U-Pb and $^{40}\text{Ar}/^{39}\text{Ar}$ evidence for overprinting of the Brasília belt by the Ribeira Belt tectonics," *Journal of the Virtual Explorer*, vol. 17, pp. 1–18, 2004.
- [113] R. S. Schmitt, R. A. J. Trouw, W. R. Van Schmus, and M. M. Pimentel, "Late amalgamation in the central part of West Gondwana: new geochronological data and the characterization of a Cambrian collisional orogeny in the Ribeira belt (SE Brazil)," *Precambrian Research*, vol. 133, no. 1-2, pp. 29–61, 2004.
- [114] M. P. S. Zuquim, R. A. J. Trouw, C. C. Trouw, and E. Tohver, "Structural evolution and U-Pb SHRIMP zircon ages of the Neoproterozoic Maria da Fé shear zone, central Ribeira belt – SE Brazil," *Journal of South American Earth Sciences*, vol. 31, pp. 199–213, 2011.
- [115] L. A. Milani, *Thermal and kinematic history and tectonic significance of the Putunã Shear Zone, southern Ribeira Belt*, MSc Dissertation, Geosciences Institute, University of São Paulo, 2020.
- [116] C. A. Salazar, C. J. Archanjo, S. W. O. Rodrigues, and M. H. B. M. Hollanda, "Age and magnetic fabric of the Três Córregos granite batholith: evidence for Ediacaran transtension in the Ribeira belt (SE Brazil)," *International Journal of Earth Sciences*, vol. 102, no. 6, pp. 1563–1581, 2013.
- [117] F. M. Faleiros and M. Pavan, *Geology and mineral resources of the Eldorado Paulista Sheet- SG.22-X-B-VI, 1:100,000 scale, São Paulo and Paraná States*, Geological Survey of Brazil – CPRM, Geology of Brazil Program – Basic Surveys, 2013.
- [118] S. Oriolo, P. Oyhantçabal, K. Wemmer et al., "Timing of deformation in the Sarandí del Yí shear zone, Uruguay: implications for the amalgamation of western Gondwana during the Neoproterozoic Brasiliano-Pan-African Orogeny," *Tectonics*, vol. 35, pp. 754–771, 2016.
- [119] S. Oriolo, P. Oyhantçabal, K. Wemmer et al., "Shear zone evolution and timing of deformation in the Neoproterozoic transpressional Dom Feliciano Belt, Uruguay," *Journal Structural Geology*, vol. 92, pp. 59–78, 2016.
- [120] P. Oyhantçabal, S. Siegesmund, K. Wemmer, and C. W. Passchier, "The transpressional connection between Dom Feliciano and Kaoko belts at 580–550 Ma," *International Journal of Earth Sciences*, vol. 100, pp. 379–390, 2011.
- [121] B. Goscombe, D. Gray, R. Armstrong, D. A. Foster, and J. Vogl, "Event geochronology of the Pan-African Kaoko Belt, Namibia," *Precambrian Research*, vol. 140, pp. 103.e1–103.e41, 2005.
- [122] D. R. Gray, D. A. Foster, B. Goscombe, C. W. Passchier, and R. A. J. Trouw, " $^{40}\text{Ar}/^{39}\text{Ar}$ thermochronology of the Pan-African Damara Orogen, Namibia, with implications for tectonothermal and geodynamic evolution," *Precambrian Research*, vol. 150, pp. 49–72, 2006.
- [123] J. Konopásek, S. Kröner, S. L. Kitt, C. W. Passchier, and A. Kröner, "Oblique collision and evolution of large-scale transcurrent shear zones in the Kaoko belt, NW Namibia," *Precambrian Research*, vol. 136, pp. 139–157, 2005.
- [124] D. L. Whitney and B. W. Evans, "Abbreviations for names of rock-forming minerals," *American Mineralogist*, vol. 95, pp. 185–187, 2010.
- [125] C. J. Archanjo, C. A. Salazar, F. P. Caltabellota, and S. W. O. Rodrigues, "The onset of the right-lateral strike-slip setting recorded in magnetic fabrics of A-type granite plutons of the Ribeira belt (SE Brazil)," *Precambrian Research*, vol. 366, article 106417, 2021.